frontiers in Earth Science

ORIGINAL RESEARCH
published: 25 March 2022
doi: 10.3389/feart.2022.845224

Nd and Sr Isotopes and REE Investigation in Tropical Weathering Profiles of Amazon Region

Adriana Maria Coimbra Horbe[1]*, *Márcio Fernando Dos Santos Albuquerque*[2] and *Elton Luiz Dantas*[1]

[1]Instituto de Geociências, Brasília, Brazil, [2]Programa de Pós-Graduação, Universidade de Brasília, Campus Darcy Ribeiro, Brasília, Brazil

The exceptional development of lateritic profiles make the Amazon one of the best places to conduct a refined study on the effects of long-term tropical climate on the Earth's surface rocks. Concentrations of Nd and Sr isotopes, as well as rare earth elements (REE), Sr, and other trace elements were determined in six profiles in order to shed new light into element behavior and into the processes controlling the geochemistry and the transfer of these elements among the different compartments of the critical zone. Our investigation indicates natural isotope regional pulse transformations in the Oxisol at the top of all profiles. The $\varepsilon Nd_{(t=0)}$ values of the parent rock, mottled horizon, and lateritic duricrust are radiogenic similar to the Amazon craton signature. The thick Oxisol has $\varepsilon_{Nd(t=0)}$ values which are much more radiogenic and less variable, whereas it has Zr, Th, Y, and REE in higher concentrations. These issues highlight a complex process for the Nd system, and the following possibilities are proposed to explain this behavior: formation of authigenic cerianite and/or kaolinite, penetration of low-temperature weathering solutions along zircon fractures, and some vegetation uptake. These possibilities allow keeping the more radiogenic Nd isotopes, whereas the less radiogenic Nd is released especially in the Oxisol after REE mineral(s) weathering. The Sr system contrary to that of Nd became less radiogenic along the profiles and relatively to the parent rocks content, because nearly all Sr was removed after K-Rb feldspar and mica weathering. However, a mixture return of less radiogenic Sr from plant, biogenic aerosol, and rainwater may have helped let the weathering profiles become less radiogenic. These characteristics let the Oxisol even less Sr radiogenic but still permitting to identify the general parent rocks signature. In contrast, Nd is highly fractionated in the Oxisol relative to the parent rock. Thus, the REE and Sr behavior, similar in the six profiles, does not necessarily reflect only the parent rock geochemistry, but it also depends on the multiple surficial processes typical of the critical zone: weathering, pedogenesis, plant root activity, and rainwater composition which change the inherited primary minerals isotope signatures.

Keywords: lateritic regolith, Oxisol, cerianite-(Ce), zircon, disorder kaolinite, rare earth element (REE)

OPEN ACCESS

Edited by:
Fabiano N. Pupim,
Federal University of São Paulo, Brazil

Reviewed by:
Francisco Ladeira,
State University of Campinas, Brazil
Ilya Bindeman,
University of Oregon, United States

***Correspondence:**
Adriana Maria Coimbra Horbe
ahorbe@unb.br

Specialty section:
This article was submitted to Geochemistry, a section of the journal Frontiers in Earth Science

Received: *29 December 2021*
Accepted: *21 February 2022*
Published: *25 March 2022*

Citation:
Horbe AMC, Albuquerque MFDS and Dantas EL (2022) Nd and Sr Isotopes and REE Investigation in Tropical Weathering Profiles of Amazon Region. Front. Earth Sci. 10:845224. doi: 10.3389/feart.2022.845224

1 INTRODUCTION

Up to 30% of the continental surface in low relief landscapes in tropical regions have developed deep weathering lateritic profiles from the basement rock (Tardy and Roquin 1998). The formation of lateritic profiles causes chemical elements and solution transfer, residual minerals accumulation (e.g. zircon and rutile), and supergene phases formation. This generates clays (e.g., kaolinite), Al and Fe oxi-hydroxides (e.g., gibbsite, hematite, and goethite), and Ti and Mn-K oxides (anatase and cryptomelane) from the parent rock to the weathering horizons (Nahon, 1991). The lateritic profile consists (from the base to the top) of a saprolite developing over the basement rock and a mottled horizon capped with a Fe-duricrust or bauxite crust. Oxisol can develop on top of the duricrust (e.g., Lucas 1997; Horbe and Costa 1999; Costa et al., 2014). Those deep weathering profiles reflect the combination of intense chemical weathering and slow physical erosion (Retallack, 2010).

During the weathering process, elements react differently, and their contents change according the parent rock, time, and weathering intensity. For instance, the rare earth elements (REE) fractionation may be controlled by different processes, such as weathering of REE-bearing minerals, physicochemical conditions, provenance differentiation, and hydraulic sorting (e.g., Henderson, 1986; Wood, 1990; Su et al., 2017; Jonell et al., 2018).

Most REE in rocks (~70–90%) are present in accessory minerals (e.g., allanite, apatite, titanite, monazite, zircon), whereas the remainders are distributed among the rock-forming minerals (Braun et al., 1993; Harlavan et al., 2009). The REE are commonly mobilized and released by weathering when hosted in phosphates (e.g., apatite) and silicates (e.g., allanite, biotite, amphibole, and plagioclase) (e.g., Hoskin and Schaltegger, 2003; Pereira et al., 2005; Laveuf and Cornu, 2009). In contrast, they accumulate when associated with residual minerals such as zircon, xenotime, monazite, thorite, and titanite (e.g., Horbe and Costa, 1999; Velbel, 1999).

The REE migrate according to their relative mobility and solubility (Laveuf and Cornu, 2009). They can be either incorporated or adsorbed into authigenic amorphous or crystalline phases (clay minerals, Fe-Mn oxyhydroxides, Al-phosphates) and organic compounds or leached out as solutes (cerianite) (Braun et al., 1993; Minarik et al., 1998; Bayon et al., 2002; Tyler, 2004; Zaitsev et al., 2011; Braun et al., 2017). Low pH and reducing conditions favor REE release from the soil and REE fractionation (Cao et al., 2001), as well as canopy interactions (Braun et al., 2017). This REE mobilization vs. accumulation behavior controls the depletion or enrichment relative to the basement rock and the formation of Ce positive anomaly (Braun et al., 1990; Ohlander et al., 1996; Tyler, 2004).

Although the weathering effect on the REE concentrations is relatively well understood, the knowledge about the effects on Nd isotope variations is not yet fully understood. For example, MacFarlane et al. (1994), McDaniel et al. (1994), Ohlander et al. (2000), Negrel et al. (2000), Viers and Wasserburg (2004), and Tripathy et al. (2011) suggest that in the natural environment, the isotope compositions are controlled by chemical and isotope signatures of REE-bearing minerals and the parent rocks. For Ohlander et al. (2000) the εNd values increase with increasing Sm/Nd ratios and with preferential adsorption of Sm relative to Nd. Ma et al. (2010) propose a Nd fractionation with preferential ^{143}Nd removal compared to ^{144}Nd. On the other hand, Liu et al. (2013), Chabaux et al. (2013), Thieblemont et al. (2014), Babechuk et al. (2015), and Moragues-Quiroga et al. (2017) relate the isotopic changes to source, atmospheric deposition, and seasonal water saturation dynamics, whereas Jonell et al. (2018) associate the changes to the grain size fractionation and mineralogy distribution. Finally, plants uptake in the upper humus-richer portion of soil profiles can fractionate REE changing the Sm-Nd isotope ratio in the soils (Andersson et al., 2001; Aubert et al., 2001).

Relative to Nd isotopes, there are much more investigations on the Sr isotopes behavior during progressive rocks weathering (e.g., Capo et al., 1998; Stewart et al., 1998; Souza et al., 2010; Wei et al., 2018). Since Sr is mostly associated with weatherable minerals (biotite, K feldspar, plagioclase, hornblende, calcite, and apatite), it is easier leached than REE and may be redistributed throughout the soil–vegetation system via cation exchange (e.g., Blum and Erel, 1997; Capo et al., 1998; Stewart et al., 1998). Therefore, the Sr isotope fractionation is more perceptible than Nd isotope fractionation, although no fractionation is expected for both in the natural environment due to their relative high atomic number and small relative mass difference (Tripathy et al., 2011). Thus, the study of Nd and Sr appears to be an extremely powerful approach for understanding the evolution of the polygenetic regolith systems (Moragues-Quiroga et al., 2017). With this goal, the present study combines mineralogical, major and trace elements, and Nd and Sr isotope analyses in order to identify the behavior and the processes controlling the REE and Sr systems in the critical zone. These information will help to better understand the transfer of elements between the different weathering lateritic profiles compartments, and to find tracers of weathering processes and element cycling. For this purpose, six lateritic profiles in the Amazon (Brazil) have been selected for study (**Figure 1**).

2 MATERIALS AND METHODS

2.1 Sampling Strategy

Six lateritic profiles, with the associated soils developed above the lateritic Fe-duricrust or Al-duricrust (bauxite), have been sampled in Central Amazon (Brazil) (**Figure 1**). These six profiles represent the effect of the critical zone on the main groups of rocks in the Amazon. Profile 1 was sampled in one open pit (Trombetas bauxite Mine), whereas profiles 2, 3, and 4 were sampled in road outcrops and 5 and 6 were sampled in boreholes (Pitinga Tin Mine) (**Figure 2**). In profiles 1, 2, and 3, developed on the same sedimentary rocks (Cretaceous Alter do Chão Formation), were sampled the weathering horizons as well as 11 samples of the parent rocks in outcrops next to the weathering profiles. In the other three profiles, only the upper part was

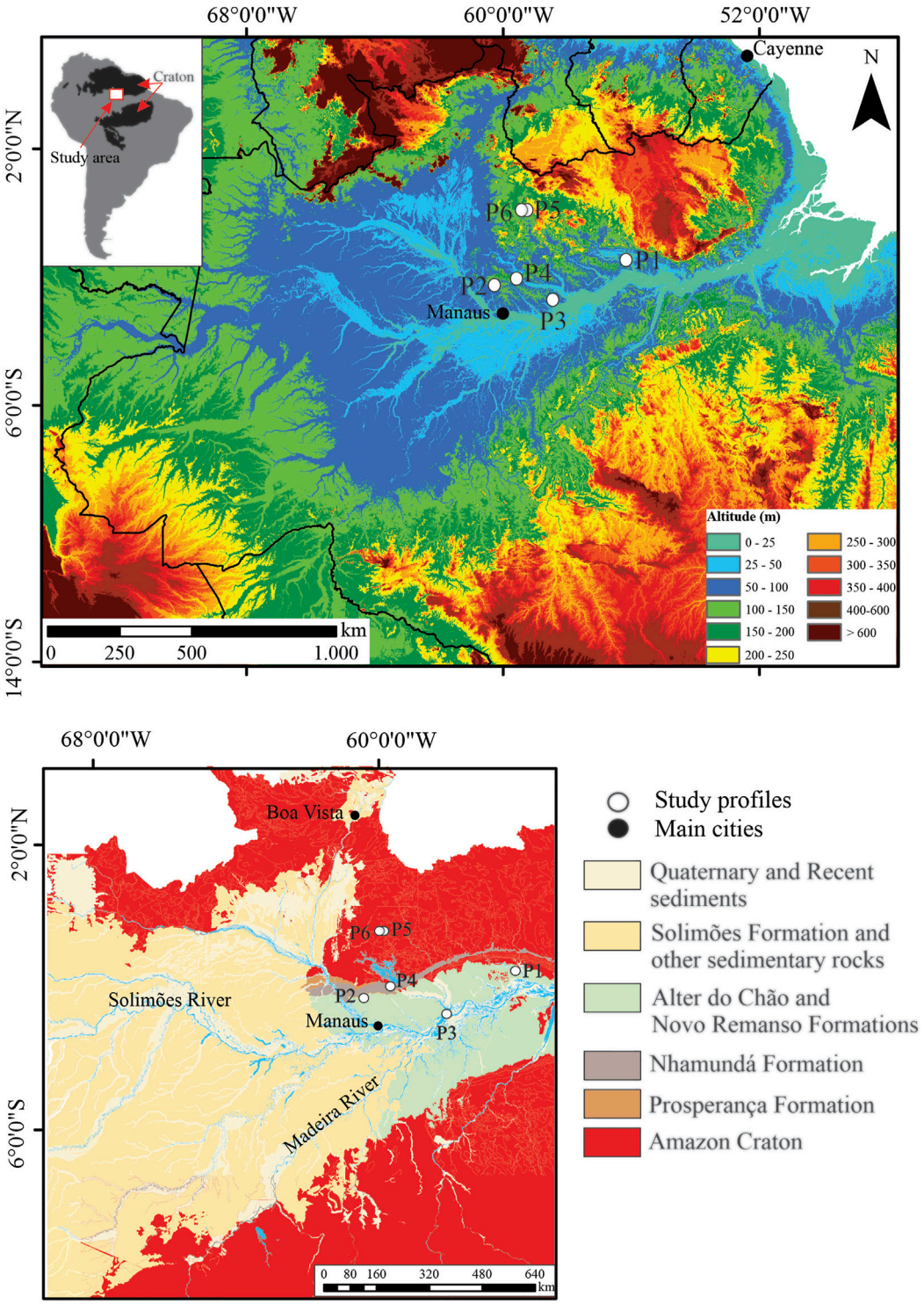

FIGURE 1 | Geographical and geological landscape of the studied region and location of the sampled profiles.

sampled because the parent rocks were not cropping out. These latest profiles allowed the complementary geochemical behavior between the lateritic duricrust and the Oxisol. Their coordinates and details about geology, geomorphology conditions, and sampled horizons are in **Table 1**.

The region has a humid tropical climate with temperatures averaging 26°C and rainfall of up to 2,100 mm/year, occurring mainly from November to May. All profiles are in areas well preserved, close to or under the dense forest vegetation, with low anthropic effect.

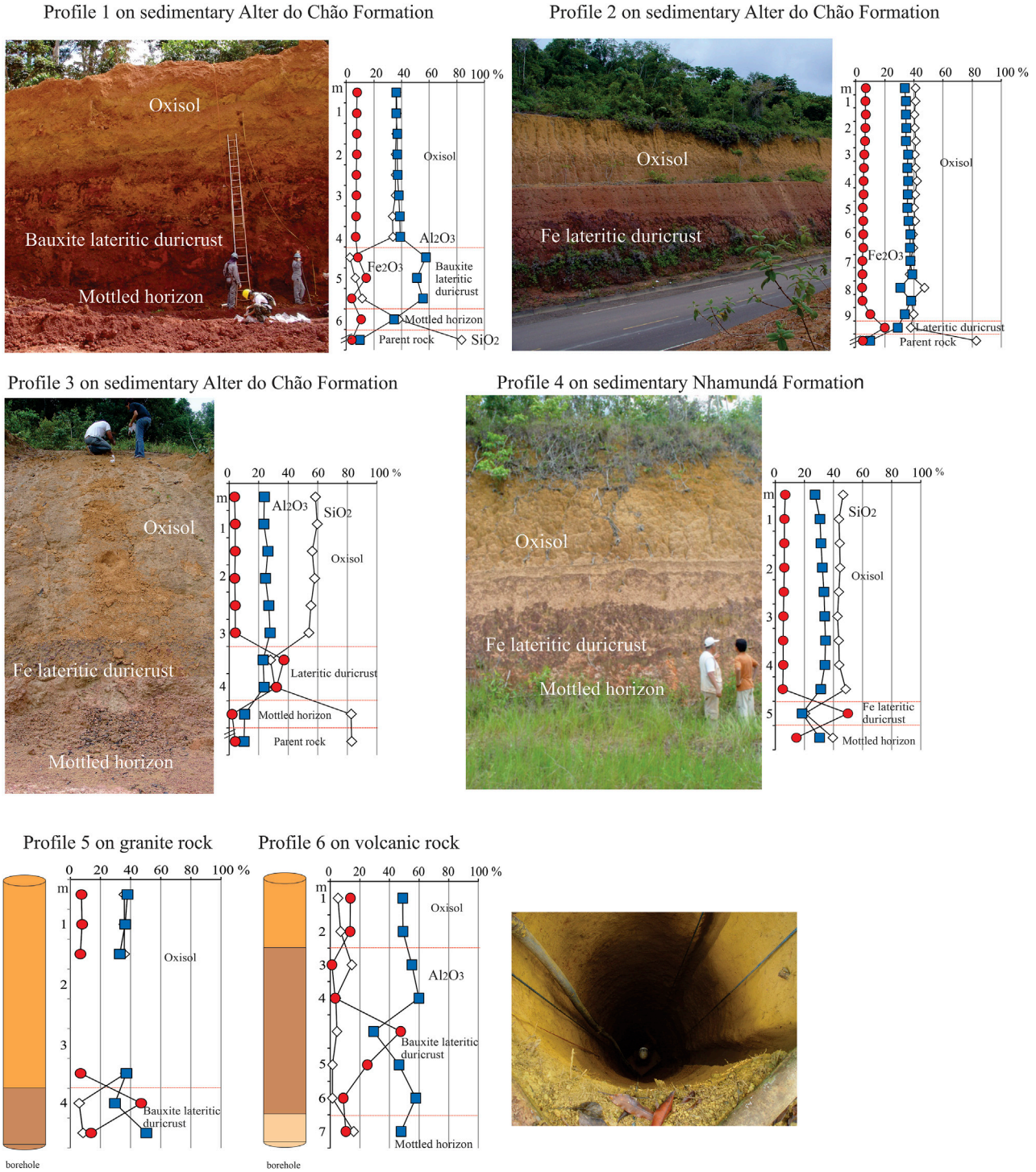

FIGURE 2 | Profile structure showing the sampled horizons and the respective plot of SiO_2, Fe_2O_3, and Al_2O_3 contents expressed as weight % along the horizons.

2.2 Profile Characteristics

Profiles 1, 2, and 3 were developed on Cretaceous sedimentary rocks (Alter do Chão Formation; Daemon and Contreiras, 1971; Daemon, 1975; Cunha et al., 1994; Silva et al., 2003) (**Figure 1**), and profile 4 on Early Silurian sedimentary rock (Cunha et al., 1994). Profiles 5 and 6 were developed on granite and felsic volcanic rocks, respectively, of the Tapajós-Parima province (2.04–1.86 Ga) from the Amazon craton (Santos et al., 2000; Santos, 2003).

The sampled horizons of the profiles are as follows (**Figure 2**): profile 1—the mottled horizon, 2 m of bauxite lateritic duricrust

TABLE 1 | Main characteristics of the study profiles and samplings.

	Profile 1	Profile 2	Profile 3	Profile 4	Profile 5	Profile 6
Parent rock	Sedimentary	Sedimentary	Sedimentary	Sedimentary	Granite	Volcanic
Geological unit	Alter do Chão Formation			Nhamundá Formation	Mapuera Group, Amazon craton	
Age	Cretaceous			Early Silurian	1.8 to 1.9 Ga	
Altitude	Up to 160 m altitude	Up to 110 m altitude	Up to 50 m altitude	Up to 110 m altitude	230 m altitude	260 m altitude
			Sampled horizons			
Oxisol	X	X	X	X	x	x
Lateritic duricrust	X	X	X	X	x	x
Mottled	X		X	X		x
Parent rock	X	X	X			

covered by 3.5 m of Oxisol; profile 2—the 0.5 m of ferruginous lateritic duricrust covered by 9 m of Oxisol; profiles 3 and 4—a mottled horizon, 1 and 2 m of ferruginous lateritic duricrust covered by 3 and 4.5 m of Oxisol, respectively; profile 5—at least 1.5 m of bauxite lateritic duricrust covered by 3.5 m of Oxisol; profile 6—a mottled horizon, the thickest bauxite lateritic crust (4 m) covered only by 2 m of Oxisol.

The mottled horizon (profiles 1, 3, 4, and 6) consists of a friable white to yellow clayey material composed mainly of kaolinite with less goethite, hematite, and variable quartz content. The lateritic duricrusts of the profiles are hard and porous with some friable and clayey portions; often it is massive to pisolith with micro- to cryptocrystalline texture and colored red to pink when bauxite, and red to brown when ferruginous (**Figure 2**). The lateritic duricrust of profiles 1, 5, and 6 is bauxitic formed mainly of gibbsite, while those of profiles 2 to 4 are ferruginous formed of hematite, goethite, quartz, and less gibbsite and anatase. Profile 2 shows some gibbsite pockets in the ferruginous duricrust.

The Oxisol covering the bauxite and the ferruginous lateritic duricrusts in all six profiles, between 2 and 9 m thick, is very homogeneous with clayey to sandy–clayey texture and no visible stratification and, sometimes, accumulates some loose bauxite and ferruginous pisoliths depending on whether they are covering bauxite and/or ferruginous lateritic duricrust. The silt and clay fractions, composed mainly of kaolinite, have minor amounts of gibbsite (profiles 1, 2, 5, and 6). The sand fraction is a mix of quartz grains, Fe oxi-hydroxide ooliths, and hard kaolinite fragments. The Oxisol in profiles 1, 5, and 6 on the bauxitic laterite duricrust has more gibbsite than the other profiles. More details about mineralogy and chemistry of profiles 1, 5, and 6 can be found in Boulangé and Carvalho, (1997), Lucas (1997), Horbe and Costa (1999), Horbe (2011), and Horbe and Anand (2011).

2.3 Analytical Procedures

Sixty-seven samples were collected from the profiles at approximately 0.5-m intervals and 11 samples from the parent rocks of profiles 1 to 3. Following air-drying and powdering, each bulk sample was subsequently submitted to chemical and isotopic analyses. For the chemical analysis, a sub-sample of 0.2 g from each sample was fused at 1,000°C with lithium meta and tetraborate for 1 h, followed by digestion with HNO_3. The resulting solution was analyzed by ICP-AES (inductively coupled plasma atomic emission spectrometer) to obtain total SiO_2, Al_2O_3, Fe_2O_3, TiO_2, and P_2O_5. Another 0.2 g sub-sample was digested in two stages with HCl, $HClO_4$, and HF for determining Hf, Nb, Rb, Sr, Ta, Th, Y, Zr, and REE with ICP-MS (inductively coupled plasma mass spectrometer). The analyses were performed at the Acme Analytical Laboratories LTD, in Canada.

A second sampling was conducted in profiles 1 and 2 to collect zircon grains from the parent rock, the lateritic duricrust, and the Oxisol due to the possible relationship between zircon, REE, and Nd isotope composition. Electron microprobe analysis (EMPA, JEOL JXA 8230) was performed at Universidade de Brasília, in Brazil in 61 zircons grains, after carbon metallization.

The isotope analyses following two procedures were performed at Laboratório de Estudos Geodinâmicos e Geocronológicos of Universidade de Brasília, in Brazil. In the first procedure, a 40–60 mg sub-sample from each sample was totally digested in two steps in the clean room environment, using a mixture of ultrapure HF/HNO_3 and 6 N HCl on a hot plate according to Gioia and Pimentel (2000). In the second procedure, a 40–60 mg sub-sample from profile 1 was digested in two steps in a clean room environment using aqua regia on a hot plate (Santoro et al., 2017). This leaching procedure digestion using aqua regia was done to determine the REE isotope composition of the exchangeable ions, colloidal, iron oxyhydroxides, and organic compounds in the leaching solution of the samples relative to the isotopes signature of the totally digested samples composed mainly of Si-Al and residual minerals.

The AG 50W-X8 cation-exchange resin was used to concentrate and separate REE. Neodymium and Sm were further separated from the REE fraction on a second AG50-X2 cation-exchange column as NH4+ using α-hydroxyisobutyric acid (α-HIBA) buffered at pH 4.5. Also, we used an Eichrom Sr-Spec® cation-exchange resin to separate the Sr isotopes. The Nd concentrates were loaded on double rhenium filaments with H_3PO_4 (0.1 M) and Sr concentrates on a tungsten filament using a TaF-solution; both were measured as metal on a Thermal Ionization Mass Spectrometer (TRITON), following Gioia and Pimentel (2000). The blank level was 100 pg, and the reproducibility was verified using the NBS 987 Sr standard (0.71028 ± 2). The measured $^{143}Nd/^{144}Nd$ ratios are presented as fractional deviations in parts per 10^4 (units) from $^{143}Nd/^{144}Nd$ in a chondritic uniform reservoir (CHUR) as measured at the present day: $\varepsilon Nd_{(t=0)} = [(^{143}Nd/^{144}Nd)_S/I_{CHUR}(0) - 1] \times 0^4$ where $(^{143}Nd/^{144}Nd)_S$ is the present-day ratio measured in the sample, and $I_{CHUR}(0)$ is the $^{143}Nd/^{144}Nd$ ratio in the CHUR reference reservoir at the present ($I_{CHUR}(0) = 0.512638$; Jacobsen and Wasserburg, 1980). The $^{143}Nd/^{144}Nd$ ratios were normalized

TABLE 2 | Chemical composition and trace element ratios.

Horizon	Depth (m)	SiO_2	Al_2O_3	Fe_2O_3	TiO_2	P_2O_5	Zr	Hf	Th	Nb	Ta	Y	Sr	Rb	Th/Nb	Nb/Y	Zr/Th	Zr/Y	Th/Y	Sr/Rb
Profile 1																				
Oxisol	0.5	36.20	36.11	7.68	3.10	0.03	1285	37	60	82	6.1	22	15	0.5	0.7	4	21	58	3	0.03
	1	36.56	35.94	7.46	3.06	0.03	1235	34	64	81	6.4	22	14	0.4	0.8	4	19	56	3	0.03
	1.5	36.09	36.88	7.54	3.17	0.03	1314	38	67	83	6.4	23	14	0.4	0.8	4	20	56	3	0.03
	2	35.56	36.76	7.39	3.14	0.02	1272	35	67	85	6.8	23	13	0.4	0.8	4	19	55	3	0.03
	2.5	35.56	37.15	7.23	3.20	0.03	1270	35	69	85	6.6	22	13	0.3	0.8	4	18	57	3	0.02
	3	35.48	37.83	7.15	3.26	0.03	1375	39	71	89	6.8	25	12	0.3	0.8	4	19	56	3	0.03
	3.5	33.36	38.71	6.95	3.13	0.02	1312	36	64	86	6.2	20	11	0.2	0.7	4	20	64	3	0.02
	4	33.62	38.87	6.82	3.33	0.03	1363	38	70	90	6.7	22	10	0.2	0.8	4	20	62	3	0.02
Duricrust	4.5	2.61	57.48	8.27	1.32	<0.01	510	14	30	34	2.4	9	3	1.2	0.9	4	17	58	3	0.38
	5	6.39	51.09	14.21	0.73	0.01	287	8	19	18	1.4	5	2	0.6	1.0	4	16	59	4	0.40
	5.5	11.30	55.54	3.82	0.72	<0.01	314	9	13	19	1.5	5	2	0.3	0.7	4	24	63	3	0.15
Mottled	6	37.98	34.40	10.76	1.69	0.01	1054	29	40	64	4.0	13	18	2.3	0.6	5	27	79	3	0.13
Parent rock average		82.85	8.84	3.69	0.40	0.05	221	6	12	13	0.9	12	38	12.0	1.0	1	23	20	1	3.78
Profile 2																				
Oxisol	0.5	41.09	33.52	6.84	1.84	0.03	1107	31	47	54	3.6	14	22	0.4	0.9	4	24	78	3	0.02
	1	40.92	34.31	6.70	1.82	0.02	1277	35	48	54	3.4	15	19	0.3	0.9	4	27	87	3	0.02
	1.5	40.32	34.45	6.78	1.79	0.03	1113	31	46	52	3.4	14	18	0.3	0.9	4	24	78	3	0.02
	2	40.55	34.53	6.51	1.80	0.02	1189	32	46	53	3.3	16	18	0.3	0.9	3	26	73	3	0.02
	2.5	41.24	34.47	6.36	1.69	0.02	1141	32	46	51	3.3	14	17	0.3	0.9	4	25	79	3	0.02
	3	40.45	35.99	5.76	1.67	0.02	1118	33	42	48	3.1	13	14	0.3	0.9	4	26	89	3	0.02
	3.5	41.09	35.45	5.57	1.60	0.01	1254	33	43	48	3.2	15	14	0.2	0.9	3	29	84	3	0.01
	4	41.94	35.88	5.23	1.58	0.01	1131	31	44	48	3.2	13	13	0.5	0.9	4	26	86	3	0.04
	4.5	40.78	35.55	5.29	1.56	0.02	1153	31	43	48	2.8	12	14	0.2	0.9	4	27	95	4	0.01
	5	40.05	35.45	4.91	1.49	0.02	1124	32	41	45	2.9	11	12	0.5	0.9	4	28	98	4	0.04
	5.5	40.85	36.22	5.05	1.55	0.02	1221	32	44	47	3.0	12	13	0.7	0.9	4	28	103	4	0.06
	6	39.13	37.35	5.09	1.56	0.01	1142	31	44	46	3.1	12	13	0.2	0.9	4	26	95	4	0.02
	6.5	39.52	37.28	4.95	1.57	0.01	1132	31	46	47	3.0	15	13	0.2	1.0	3	25	77	3	0.02
	7	37.68	37.56	4.58	1.56	<0.01	1316	38	41	47	3.7	12	11	0.3	0.8	4	32	108	3	0.03
	7.5	36.91	38.82	4.52	1.51	0.01	1221	34	41	47	3.0	12	11	0.2	0.9	4	30	103	3	0.02
	8	47.19	30.56	4.38	1.33	0.04	1471	40	33	51	3.0	32	67	1.8	0.7	2	44	45	1	0.03
	8.5	38.28	38.07	4.56	1.57	<0.01	1382	38	44	47	3.2	12	11	0.3	0.9	4	31	118	4	0.03
	9	39.82	33.52	9.79	1.34	0.01	1317	36	53	39	2.5	11	10	0.3	1.3	3	25	118	5	0.03
Duricrust	9.5	37.64	28.69	19.90	0.77	0.03	571	15	16	28	1.8	9	15	2.2	0.6	3	35	61	2	0.15
Parent rock average		82.85	8.84	3.69	0.40	0.05	221	6	12	13	0.9	12	38	12.0	1.0	1	23	20	1	3.78
Profile 3																				
Oxisol	0.5	58.44	23.80	3.64	1.83	0.04	2483	62	28	43	2.6	28	19	<0.1	0.6	2	90	89	1	0.01
	1	59.64	23.44	4.09	1.57	0.03	2180	53	29	39	2.4	25	22	0.5	0.8	2	74	86	1	0.02
	1.5	56.22	26.27	4.09	1.99	0.03	2605	63	33	49	3.0	28	24	<0.1	0.7	2	79	91	1	0.00
	2	57.86	24.57	3.75	1.88	0.04	2853	71	33	47	2.8	29	22	0.5	0.7	2	86	97	1	0.02
	2.5	55.35	26.82	4.12	2.07	0.04	2783	68	36	49	2.9	31	23	<0.1	0.7	2	77	89	1	0.00
	3	53.99	27.71	4.17	2.19	0.03	2907	71	34	52	3.2	33	25	0.5	0.6	2	86	89	1	0.02
Duricrust	3.5	27.97	23.01	37.04	0.89	0.06	1056	26	44	21	1.6	10	13	1.2	1.5	3	24	100	4	0.09
	4	30.97	23.70	32.04	1.77	0.07	1595	40	39	42	2.4	31	29	<0.1	0.9	1	41	52	1	0.00
Mottled	4.5	82.48	10.44	1.96	0.84	0.04	1049	27	17	21	1.3	13	20	0.9	0.8	2	62	79	1	0.05
Parent rock average		82.85	8.84	3.69	0.40	0.05	221	6	12	13	0.9	12	38	12.0	1.0	1	23	20	1	3.78
Profile 4																				
Oxisol	0.5	46.57	27.32	6.82	1.64	0.04	1639	44	32	41	2.8	21	30	0.7	0.8	2	52	78	2	0.02
	1	43.76	30.69	6.29	1.68	0.04	1616	43	32	45	2.9	18	28	0.4	0.7	2	50	89	2	0.01
	1.5	44.29	31.35	6.19	1.65	0.04	1726	44	34	44	3.2	18	28	0.2	0.8	2	50	95	2	0.01
	2	44.57	32.31	6.16	1.70	0.04	1826	46	34	44	3.3	20	26	0.3	0.8	2	53	90	2	0.01
	2.5	43.67	33.46	5.80	1.62	0.02	1585	45	44	42	2.8	17	24	1.7	1.0	3	36	94	3	0.07
	3	42.71	33.99	5.55	1.52	0.03	1623	44	32	38	2.5	16	23	0.4	0.8	2	50	100	2	0.02
	3.5	43.64	34.51	5.34	1.56	0.04	1507	42	30	40	2.7	15	21	0.4	0.8	3	50	103	2	0.02
	4	43.97	34.09	5.45	1.60	0.03	1695	45	31	39	2.5	15	20	0.6	0.8	3	55	112	2	0.03
	4.5	48.39	31.25	5.12	1.40	0.04	1588	44	31	38	2.7	19	19	0.9	0.8	2	51	82	2	0.05

(Continued on following page)

TABLE 2 | (*Continued*) Chemical composition and trace element ratios.

Horizon	Depth (m)	SiO_2	Al_2O_3	Fe_2O_3	TiO_2	P_2O_5	Zr	Hf	Th	Nb	Ta	Y	Sr	Rb	Th/Nb	Nb/Y	Zr/Th	Zr/Y	Th/Y	Sr/Rb
Duricrust	5	20.37	18.39	49.86	0.55	0.06	495	13	53	15	0.9	5	5	0.2	3.5	3	9	108	10	0.04
Mottled	5.5	39.56	30.44	14.47	1.17	0.04	1003	26	38	32	2.2	12	17	0.7	1.2	3	26	85	3	0.04
Profile 5																				
Oxisol	0.5	35.76	32.79	6.65	1.59	0.03	2486	102	280	375	24	68	14	<0.1	0.7	6	9	36	4	—
	1	35.91	36.41	7.75	1.78	0.02	2531	—	325	441	—	95	16	<0.1	0.7	5	8	27	3	—
	1.5	35.83	37.90	7.35	1.78	0.02	3628	145	335	434	35	92	15	<0.1	0.8	5	11	40	4	—
	3.5	36.82	37.20	6.79	1.59	<0.01	2219	103	294	443	41	87	12	<0.1	0.7	5	8	26	3	—
Duricrust	4	5.85	29.57	46.96	0.32	0.04	512	26	319	151	12	21	2	0.6	2.1	7	2	24	15	0.32
	4.5	8.42	50.39	13.74	0.27	<0.01	445	25	127	181	17	29	3	1.1	0.7	6	4	15	4	0.33
Profile 6																				
Oxisol	1	5.24	48.93	13.60	3.62	0.10	3757	104	152	147	10.0	100	1	1.1	1.0	1	25	38	2	1.45
	2	6.98	49.11	13.38	3.54	0.10	3596	100	156	146	10.0	101	83	2.1	1.1	1	23	36	2	0.03
Duricrust	3	14.6	55.12	1.14	1.02	<0.01	634	18	24	27	1.9	9	12	2.0	0.9	3	26	70	3	0.17
	4	3.82	59.88	3.37	1.32	0.03	1122	32	55	54	3.9	38	29	0.1	1.0	1	20	30	1	0.003
	4.5	4.54	29.27	47.55	0.94	0.05	716	19	57	38	2.6	39	19	4.0	1.5	1	13	18	1	0.21
	5	1.54	46.43	25.04	1.03	0.06	865	26	53	44	2.8	40	45	1.8	1.2	1	16	22	1	0.04
	6	1.48	57.76	8.80	1.24	0.22	1001	28	66	61	4.1	66	165	1.2	1.1	1	15	15	1	0.01
Mottled	7	15.79	47.79	10.54	1.46	0.30	1137	32	81	65	4.7	83	208	6.5	1.2	1	14	14	1	0.03

Oxides expressed as wt% and trace elements as ppm.

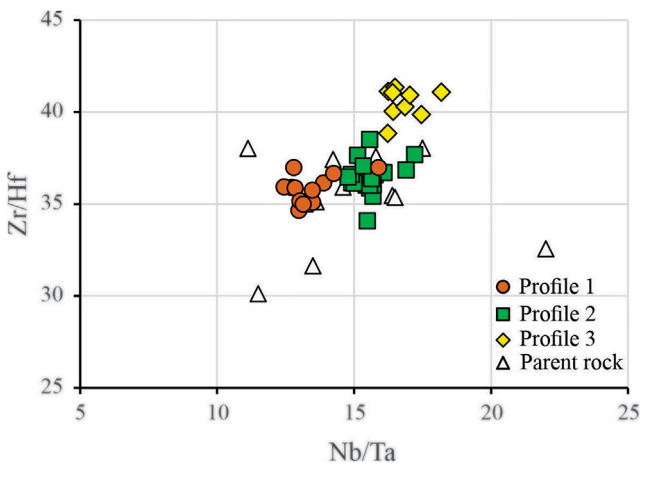

FIGURE 3 | Plot of Zr/Hf *vs*. Nb/Ta ratios of the bulk samples showing the range among the parent rock and the horizons of profiles 1 and 2.

to $^{146}Nd/^{144}Nd$ of 0.7219 for a decay constant (λ) of 6.54×10^{-12} $year^{-1}$.

3 RESULTS

3.1 Bulk Geochemistry

In general, the parent rock, the mottled horizon, and the Oxisol show low Fe_2O_3 compared to the lateritic duricrust (**Figure 2**; **Table 2**). The lateritic duricrusts may have either high Fe_2O_3 or high Al_2O_3, depending on whether they are more ferruginous (profiles 2, 3, and 4) or bauxitic (profiles 1, 5, and 6). The similar SiO_2 and Al_2O_3 contents in the Oxisol in profiles 1, 3, and 5 (**Figure 2**) are related to the coexistence of quartz, kaolinite, and gibbsite; the highest Al_2O_3 content in profile 6 is related to the predominance of kaolinite in the mottled horizon and of gibbsite in the Oxisol, and the highest SiO_2 content in profiles 3 and 4 is related to the predominance of quartz along the profiles.

In all profiles, the Hf, Nb, Ta, Th, TiO_2, Y, and Zr concentrations are higher in the Oxisol (**Table 2**). There are some chemical variabilities among the parent rock, the mottled horizon, and the lateritic duricrust. For example, in the high Th and Fe_2O_3 in samples 3.5 and 5 m of profiles 3 and 4, respectively, the Th/Nb and Th/Y ratios are also high. There is also high SiO_2, Zr, and Y content in sample 8 m of profile 2. Despite these variabilities, the Th/Nb, Nb/Y, Zr/Th, Zr/Y, and Th/Y ratios along the profiles are very similar, and the Zr/Hf and Nb/Ta ratios of profiles 1, 2, and 3 are in the range of the parent rock variability (**Figure 3**).

The REE concentrations are higher in the parent rock (profiles 1, 2, and 3) and in the mottled horizon (profile 6) relative to the upward horizons of the respective profiles (**Table 3**). On the other hand, the REE in the mottled horizon of profiles 5 and 6 and in most samples of the lateritic duricrust and Oxisol of all profiles follow the Zr and TiO_2 concentrations (**Tables 2**, **3**) that are higher in the Oxisol than in the downward horizons. The P_2O_5 content along the profiles follow the REE concentration only in the parent rock of profiles 1 and 2 and in the mottled horizon of profile 6.

3.2 Normalization Relative to the Upper Continental Crust and Lateritic Duricrust

The REE concentrations in the samples were normalized to the upper continental crust (UCC, Taylor and McLenann, 1985) and to the average of the respective lateritic duricrust (**Figures 4**, **5**) of

TABLE 3 | REEs concentration expressed as ppm and isotope ratios.

Depth (m)	La	Ce	Pr	Nd	Sm	Eu	Gd	Tb	Dy	Ho	Er	Tm	Yb	Lu	REE	$^{147}Sm/^{144}Nd$	$^{143}Nd/^{144}Nd$, ±2SE	εNd (0)	$T_{DM\ (Ga)}$	$^{87}Sr/^{86}Sr$, ±2SE
Profile 1																				
0.5	12.6	22.2	2.26	8.2	1.43	0.33	1.74	0.40	2.93	0.75	2.75	0.51	3.88	0.64	60.62	0.1227	0.511933 ± 10	−13.76	1.85	0.71530 ± 1
1	11.8	21.3	2.12	8.2	1.40	0.32	1.71	0.39	2.76	0.76	2.63	0.47	3.74	0.64	58.24	0.1252	0.511904 ± 9	−14.32	1.95	–
1.5	11.7	21.5	2.14	7.9	1.52	0.33	1.73	0.41	3.12	0.76	2.89	0.50	4.00	0.70	59.20	0.1231	0.511908 ± 6	−14.24	1.89	0.70962 ± 1
2	11.3	20.1	2.06	7.7	1.51	0.32	1.79	0.39	3.06	0.79	2.73	0.51	3.80	0.67	56.73	0.1287	0.511934 ± 10	−13.72	1.97	0.71560 ± 1
2.5	11.0	19.9	1.99	7.5	1.35	0.32	1.67	0.40	2.93	0.74	2.83	0.52	3.81	0.66	55.62	0.1273	0.511920 ± 14	−14.01	1.97	–
3	10.7	19.2	1.92	6.8	1.51	0.31	1.73	0.43	3.20	0.82	2.97	0.54	4.21	0.73	55.07	0.1622	0.511920 ± 26	−14.00	3.40	–
3.5	9.5	17.6	1.76	6.5	1.31	0.28	1.51	0.36	2.73	0.68	2.60	0.46	3.77	0.67	49.73	0.1341	0.511940 ± 5	−13.61	2.10	0.71515 ± 1
4	9.5	17.8	1.79	6.2	1.31	0.30	1.59	0.38	2.88	0.76	2.79	0.50	3.94	0.70	50.44	–	0.511934 ± 16	−13.74	–	0.71518 ± 1
4.5	5.6	8.0	0.65	2.2	0.51	0.10	0.66	0.15	1.17	0.32	1.18	0.20	1.64	0.28	22.66	0.1465	0.511673 ± 30	−18.83	3.14	
5	3.7	5.2	0.43	1.3	0.31	0.06	0.36	0.09	0.62	0.17	0.63	0.11	0.92	0.15	14.05	0.1235	0.511523 ± 21	−21.75	2.56	0.71594 ± 2
5.5	7.8	8.6	0.62	1.7	0.28	0.05	0.34	0.09	0.60	0.18	0.63	0.11	0.93	0.17	22.10	0.1194	0.511694 ± 14	−18.41	2.17	0.71480 ± 3
6	33.9	36.0	2.70	7.3	0.91	0.20	1.03	0.23	1.90	0.43	1.62	0.31	2.42	0.43	89.38	0.0994	0.511623 ± 5	−19.80	1.88	
Parent rock average	41.0	77.22	6.14	20.97	2.92	0.52	2.32	0.37	2.12	0.44	1.30	0.21	1.48	0.24	157.24			See **Table 4**		
Profile 2																				
0.5	18.7	23.6	2.79	9.3	1.51	0.32	1.37	0.28	1.89	0.49	1.65	0.31	2.49	0.44	65.14	0.1067	0.511818 ± 18	−16.00	1.73	0.71762 ± 1
1	18.8	22.9	2.77	9.9	1.38	0.29	1.37	0.30	1.88	0.49	1.81	0.35	2.67	0.47	65.38	0.1018	0.511830 ± 8	−15.76	1.64	0.70860 ± 1
1.5	18.4	23.2	2.70	9.2	1.38	0.29	1.33	0.28	1.98	0.49	1.74	0.32	2.48	0.43	64.22	0.1005	0.511843 ± 15	−15.51	1.60	–
2	17.9	22.3	2.58	8.5	1.37	0.30	1.39	0.30	2.17	0.57	1.96	0.37	2.71	0.48	62.90	0.1004	0.511824 ± 16	−15.88	1.67	0.71978 ± 1
2.5	17.7	20.7	2.45	8.0	1.28	0.28	1.26	0.27	1.96	0.48	1.76	0.32	2.54	0.44	59.44	0.1000	0.511708 ± 23	−18.15	1.78	–
3	15.6	18.5	2.19	6.9	1.16	0.24	1.07	0.23	1.64	0.41	1.60	0.30	2.38	0.44	52.66	0.1005	0.511981 ± 28	−12.87	1.42	0.72443 ± 1
3.5	15.7	18.2	2.16	6.7	1.11	0.24	1.18	0.26	1.87	0.50	1.75	0.35	2.72	0.45	53.19	0.1004	0.511820 ± 9	−15.97	1.63	0.72065 ± 1
4	15.1	17.3	2.07	6.8	1.18	0.23	1.17	0.24	1.70	0.43	1.62	0.30	2.31	0.42	50.87	0.1034	0.511792 ± 10	−16.51	1.72	0.72093 ± 1
4.5	15.6	17.8	2.10	6.9	1.08	0.24	1.01	0.22	1.58	0.42	1.53	0.28	2.36	0.41	51.53	0.0988	0.511732 ± 7	−17.67	1.73	
5	14.7	16.2	1.97	6.3	1.05	0.23	0.99	0.21	1.56	0.39	1.47	0.28	2.17	0.38	47.90	0.1004	0.511850 ± 9	−15.37	1.59	0.72312 ± 1
5.5	15.0	16.8	2.01	5.9	0.99	0.22	1.00	0.22	1.51	0.39	1.48	0.27	2.20	0.40	48.39	0.1033	0.511858 ± 40	−15.22	1.62	0.72050 ± 4
6	15.1	16.9	2.05	6.4	1.05	0.23	1.01	0.22	1.61	0.41	1.44	0.27	2.34	0.39	49.42	0.0989	0.511752 ± 12	−17.28	1.70	0.73021 ± 1
6.5	15.5	16.8	2.01	6.5	1.03	0.21	1.10	0.26	1.83	0.50	1.75	0.32	2.47	0.44	50.72	0.1000	0.511776 ± 10	−16.81	1.69	0.72229 ± 1
7	13.7	14.4	1.77	5.7	0.97	0.21	0.94	0.22	1.63	0.42	1.53	0.29	2.41	0.43	44.62	0.1016	0.511796 ± 19	−16.42	1.68	0.71415 ± 1
7.5	14.0	15.0	1.78	5.4	0.92	0.20	0.95	0.21	1.46	0.40	1.55	0.29	2.30	0.42	44.88	0.1005	0.511781 ± 8	−16.73	1.69	0.71134 ± 1
8	58.6	83.0	6.42	18.0	2.64	0.51	2.73	0.60	4.17	1.02	3.61	0.65	4.89	0.80	187.64	0.0874	0.511726 ± 12	−17.79	1.58	0.72013 ± 4
8.5	14.3	15.1	1.77	5.3	0.89	0.19	0.95	0.21	1.44	0.39	1.48	0.29	2.30	0.42	45.03	0.1012	0.511805 ± 15	−16.25	1.66	0.72266 ± 1
9	14.2	13.4	1.66	4.9	0.85	0.18	0.86	0.19	1.32	0.38	1.43	0.28	2.31	0.42	42.38	0.1042	0.511787 ± 29	−16.61	1.74	0.71451 ± 1
9.5	43.8	22.6	3.72	10.5	1.36	0.32	1.39	0.23	1.39	0.32	1.04	0.18	1.45	0.26	88.26	0.0809	0.511597 ± 17	−20.30	1.65	0.71828 ± 2
Parent rock average	41.0	77.22	6.14	20.97	2.92	0.52	2.32	0.37	2.12	0.44	1.30	0.21	1.48	0.24	157.24			See **Table 4**		
Profile 3																				
0.5	26.2	28.4	3.29	9.1	1.56	0.36	2.03	0.52	3.75	0.89	3.66	0.57	4.72	0.81	85.86	0.1080	0.511906 ± 15	−14.29	1.63	0.71662 ± 2
1	23.4	30.1	3.22	10.9	2.01	0.40	1.97	0.50	3.65	0.8	3.06	0.51	4.09	0.70	85.31	0.1054	0.511887 ± 11	−14.65	1.62	0.71956 ± 1
1.5	28.9	31.8	3.36	10.6	1.83	0.40	2.10	0.54	4.05	0.92	3.71	0.62	4.88	0.85	94.56	0.1059	0.511868 ± 12	−15.02	1.65	0.72063 ± 3
2	27.1	30.4	3.18	9.4	1.83	0.39	2.06	0.56	4.01	0.95	3.68	0.61	4.97	0.88	90.02	0.1088	0.511900 ± 8	−14.40	1.65	0.72219 ± 1
2.5	29.8	32.8	3.38	10.3	1.91	0.43	2.14	0.60	4.36	0.97	3.95	0.66	5.25	0.89	97.44	0.1089	0.511894 ± 17	−14.52	1.66	0.72050 ± 1
3	33.2	35.3	3.59	10.5	2.50	0.47	2.35	0.62	4.67	1.05	4.22	0.68	5.53	0.96	105.64	0.1103	0.511884 ± 4	−14.70	1.69	0.72107 ± 4
3.5	23.7	25.5	2.24	5.8	0.86	0.17	0.79	0.2	1.38	0.31	1.24	0.21	1.79	0.33	64.52	0.0921	0.511729 ± 13	−17.73	1.64	0.72505 ± 1
4	37.8	35.1	3.63	10.6	2.02	0.48	2.49	0.64	4.51	1.00	3.76	0.58	4.64	0.75	108.00	0.0938	0.511703 ± 9	−18.23	1.69	0.72564 ± 4
4.5	30.2	26.7	2.72	7.3	1.11	0.23	1.11	0.27	1.92	0.43	1.69	0.28	2.28	0.40	76.64	0.0895	0.511712 ± 7	−18.05	1.62	0.72485 ± 1
Parent rock average	41.0	77.22	6.14	20.97	2.92	0.52	2.32	0.37	2.12	0.44	1.30	0.21	1.48	0.24	157.24			See **Table 4**		
Profile 4																				
0.5	31.0	39.2	4.22	13.2	2.09	0.43	1.99	0.43	2.90	0.70	2.43	0.44	3.32	0.58	102.93	0.0983	0.511885 ± 22	−14.69	1.52	0.72020 ± 1
1	29.3	38.1	4.02	12.6	1.93	0.39	1.72	0.36	2.41	0.63	2.10	0.41	3.23	0.56	97.76	1.5830	0.511803 ± 18	−16.29	–	0.72029 ± 1
1.5	28.1	36.3	3.76	11.6	2.01	0.42	1.95	0.38	2.66	0.65	2.44	0.44	3.40	0.61	94.72	0.0984	0.511759 ± 16	−17.14	1.68	0.72030 ± 1
2	26.6	34.2	3.57	10.4	1.88	0.39	1.91	0.40	2.87	0.69	2.69	0.48	3.79	0.72	90.59	0.0995	0.511770 ± 5	−16.94	1.69	0.72061 ± 1
2.5	27.4	34.2	3.70	11.6	2.01	0.37	1.69	0.34	2.59	0.57	2.20	0.39	3.26	0.54	90.86	0.0975	0.511742 ± 22	−17.49	1.69	0.72223 ± 1
3	26.5	32.7	3.49	10.1	1.70	0.34	1.65	0.33	2.16	0.57	2.15	0.37	3.17	0.55	85.78	0.0984	0.511751 ± 14	−17.30	1.70	0.72149 ± 1
3.5	26.9	31.8	3.30	10.2	1.56	0.31	1.42	0.30	2.10	0.50	1.92	0.36	2.94	0.49	84.10	0.0988	0.511773 ± 7	−16.87	1.67	0.72219 ± 1
4	26.5	30.7	3.27	9.3	1.46	0.31	1.45	0.30	2.19	0.54	1.93	0.35	2.90	0.54	81.74	0.0966	0.511786 ± 9	−16.62	1.62	0.72294 ± 1
4.5	26.4	31.8	3.22	9.4	1.52	0.31	1.59	0.36	2.55	0.62	2.34	0.45	3.49	0.59	84.64	0.0968	0.511737 ± 13	−17.57	1.69	0.72379 ± 1
5	8.4	11.8	0.96	2.8	0.45	0.09	0.43	0.09	0.61	0.15	0.59	0.11	0.86	0.16	27.50	0.0947	0.511670 ± 16	−18.88	1.75	0.72524 ± 1

(Continued on following page)

TABLE 3 | (*Continued*) REEs concentration expressed as ppm and isotope ratios.

Depth (m)	La	Ce	Pr	Nd	Sm	Eu	Gd	Tb	Dy	Ho	Er	Tm	Yb	Lu	REE	$^{147}Sm/^{144}Nd$	$^{143}Nd/^{144}Nd$, ±2SE	εNd (0)	T_{DM} (Ga)	$^{87}Sr/^{86}Sr$, ±2SE
5.5	27.1	30.0	2.84	7.5	1.24	0.25	1.22	0.24	1.61	0.40	1.44	0.26	2.10	0.39	76.59	0.0914	0.511715 ± 14	−18.01	1.64	0.72614 ± 1
Profile 5																				
0.5	10.9	23.7	2.29	8.8	2.55	0.33	4.13	1.28	9.99	2.64	10.15	1.92	15.80	2.53	97.01	0.1687	0.512154 ± 21	−9.45	3.06	0.75661 ± 4
1	13.7	31.4	2.84	9.7	3.00	0.41	5.04	1.65	13.38	3.17	12.69	2.45	19.78	3.24	122.45	0.1566	0.512045 ± 8	−11.56	2.67	
1.5	12.7	27.8	2.66	10.0	3.15	0.37	5.40	1.65	13.18	3.28	12.58	2.58	20.83	3.48	119.66	0.1776	0.512129 ± 7	−9.93	–	0.76493 ± 1
2	–	–	–	7.5	2.03	–	–	–	–	–	–	–	–	–		0.1634	0.512085 ± 15	−10.78	2.93	
2.5	–	–	–	6.9	1.95	–	–	–	–	–	–	–	–	–		0.1704	0.512101 ± 11	−10.47	3.42	0.76552 ± 7
3	–	–	–	6.8	1.98	–	–	–	–	–	–	–	–	–		0.1765	0.512168 ± 12	−9.17	3.78	
3.5	12.2	29.2	2.50	8.8	2.50	0.28	4.53	1.53	12.12	2.88	11.32	2.26	17.41	2.94	110.47	0.1837	0.512137 ± 11	−9.77	–	0.76191 ± 1
4	5.1	8.8	0.76	2.4	0.60	0.06	1.03	0.29	2.66	0.67	2.81	0.58	4.57	0.85	31.18	0.1636	0.511959 ± 24	−13.24	3.37	0.73958 ± 4
4.5	2.9	5.1	0.38	1.2	0.40	<0.50	0.88	0.31	3.04	0.81	3.55	0.72	6.23	1.01	26.58	0.2080	0.512039 ± 16	−11.69	–	0.78881 ± 5
Profile 6																				
1	142.8	271.0	26.26	81.8	12.40	2.01	9.43	1.93	13.90	3.28	12.19	2.20	16.54	2.86	598.70	–	–	–	–	0.74956 ± 2
2	147.7	274.9	27.05	82.2	13.40	1.97	9.58	2.04	14.62	3.29	12.13	2.11	16.04	2.72	609.70	0.0921	0.511611 ± 3	−20.03	1.78	0.74957 ± 7
3	18.5	27.3	2.32	7.6	1.00	0.23	0.86	0.16	1.30	0.32	1.05	0.20	1.53	0.27	63.10	0.0937	0.511749 ± 6	−17.34	1.63	0.75420 ± 2
4	58.6	104.9	10.12	31.2	4.80	0.76	3.74	0.76	5.53	1.21	4.36	0.80	6.21	1.00	234.30	0.0951	0.511564 ± 20	−20.94	1.89	0.74711 ± 1
4.5	51.1	93.4	10.65	38.0	7.70	1.26	5.64	1.20	8.11	1.69	5.60	0.95	6.65	0.98	233.80	–	–	–	–	0.74706 ± 1
5	109.4	131.7	18.18	52.3	7.30	1.14	4.47	0.95	6.04	1.32	4.75	0.81	5.97	0.97	344.70	0.0843	0.511506 ± 21	−22.08	1.80	0.75413 ± 1
6	198.7	307.0	36.99	124.8	19.20	2.91	14.26	2.32	12.43	2.33	7.09	1.21	8.09	1.31	738.00	0.0975	0.511488 ± 20	−22.43	2.03	0.76083 ± 1
7	250.6	482.8	50.23	167.9	25.00	3.72	16.29	2.95	16.46	3.02	9.03	1.49	10.72	1.69	1,041.90	0.0907	0.511468 ± 15	−22.83	1.94	0.75961 ± 1

See horizons names in ***Table 2***.

the profiles to seek the weathering effect. The UCC normalized profile 5 (on granite rock) shows enrichment of heavy rare earth elements (HREE) relative to light rare earth elements (LREE) and negative Eu anomaly (**Figure 4**). Among the profiles, the UCC normalized profile 6 (on felsic volcanic rock) is the most enriched in REE, and profiles 1 to 4 (on sedimentary rocks) show slight enrichment in HREE relative to the LREE. In general, the lateritic duricrusts are less enriched in REE than the Oxisol, the mottled horizon, and the parent rock, except for the LREE of the lateritic duricrust of profiles 2 and 3 whose REE fractionation ratios are similar to the Oxisol (**Figure 4**). The parent rock of profiles 1, 2, and 3 (Alter do Chão Formation) is more enriched in LREE than most of the weathering horizon samples.

The REE patterns normalized to the lateritic duricrust indicate that the Oxisol is REE enriched (**Figure 5**), except in profile 2, in which most samples are depleted in LREE.

3.3 Chemistry of Zircon Grains of Profiles 1 and 2

Profiles 1 and 2 were chosen for a more detailed study since they are almost 500 km apart in the east-to-west direction and can provide information about some atmospheric deposition. The zircon grain shapes from these profiles varied greatly, changing from prismatic to sub-round and round, homogenous to zoned, and colored from white and translucent to gray and opaque. The zircon grains from bauxite, Fe duricrust, and Oxisol have reddish stains, while in the parent rock, 90% of the zircon grains are translucent. Several grains show fractures where low-temperature weathering solutions could penetrate (**Figure 6**).

The zircon grains have 57.63–68.25% of ZrO_2, 30 to 35 wt% of SiO_2, up to 0.9 wt% of REE_2O_3, and less than 4.3 wt% of other elements (Hf + Y + Th + U + Nb + P, all of them as oxides wt%) (**Figure 6**). There are some zircon samples out of the parent rock range because of high UO_2 and high REE as well.

3.6 Sm/Nd and Nd Isotopes

The Sm/Nd ratios are higher in the parent rock of profiles 1 to 3 and do not follow the $\varepsilon Nd_{(t=0)}$ that is usually less radiogenic in the parent rock, mottled horizon, and lateritic duricrust compared to the much more radiogenic (a drift of 1–7 $\varepsilon Nd_{(t=0)}$ units, **Figure 9**) and less variable Oxisol (**Figure 7**; **Tables 3**, **4**). However, some peculiarities should be highlighted. Sample 3 m of profile 2 shows a pulse to high radiogenic ratio ($\varepsilon Nd_{(t=0)}$ −12) relative to the other samples; profile 5 (from granite) is the most radiogenic ($\varepsilon Nd_{(t=0)}$ −13 to −9), while the other profiles are isotopically similar ($\varepsilon Nd_{(t=0)}$ −22 to −13); profile 6 (from felsic volcanic rocks), which has the thickest lateritic duricrust, became more radiogenic toward the top ($\varepsilon Nd_{(t=0)}$ −22 to −17). There is a slight displacement to more radiogenic $\varepsilon Nd_{(t=0)}$ in the Oxisol upper meter in profiles 1, 3, 4, and 5 (**Figure 7**).

The $\varepsilon Nd_{(t=0)}$ of almost all profile 1 samples, digested using aqua regia to determine the REE isotope composition of the exchangeable ions, colloidal, iron oxyhydroxides, and organic compounds relative to the isotopes signature of the totally

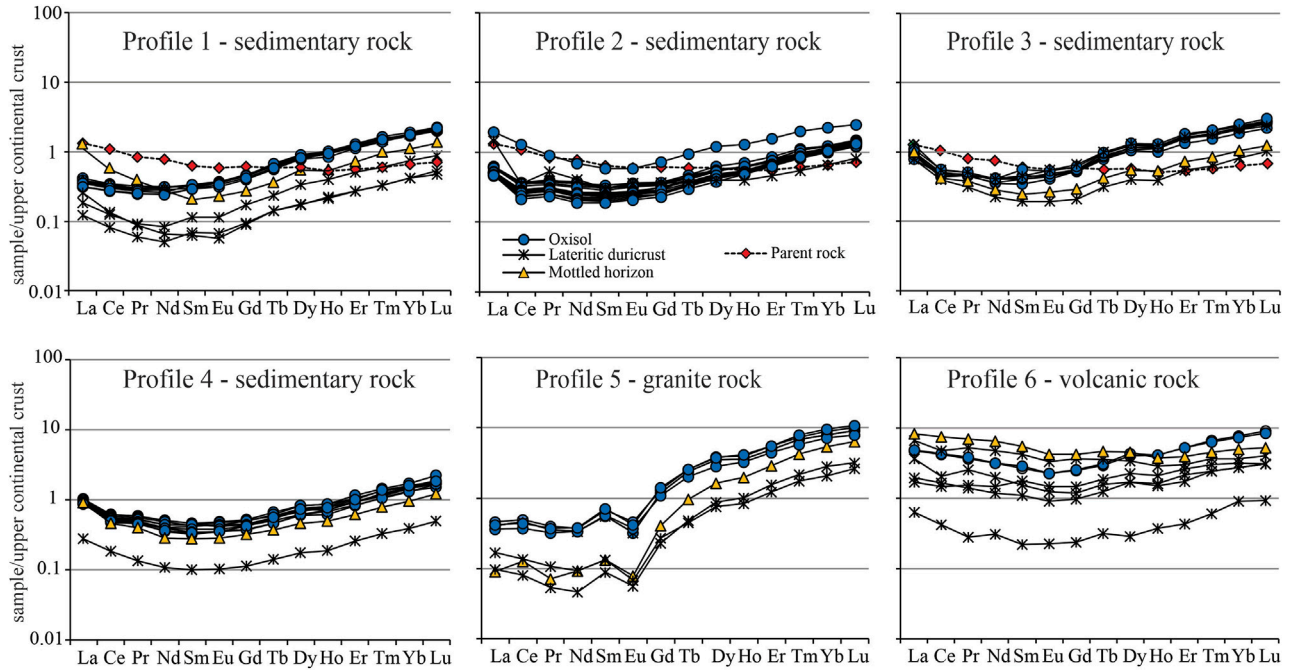

FIGURE 4 | Plot of REE expressed as ppm normalized to the estimated average composition of upper continental crust (UCC) of Taylor and McLenann (1985). In general, the lateritic duricrusts are less enriched in REE than the Oxisol, the mottled horizon, and the parent rock.

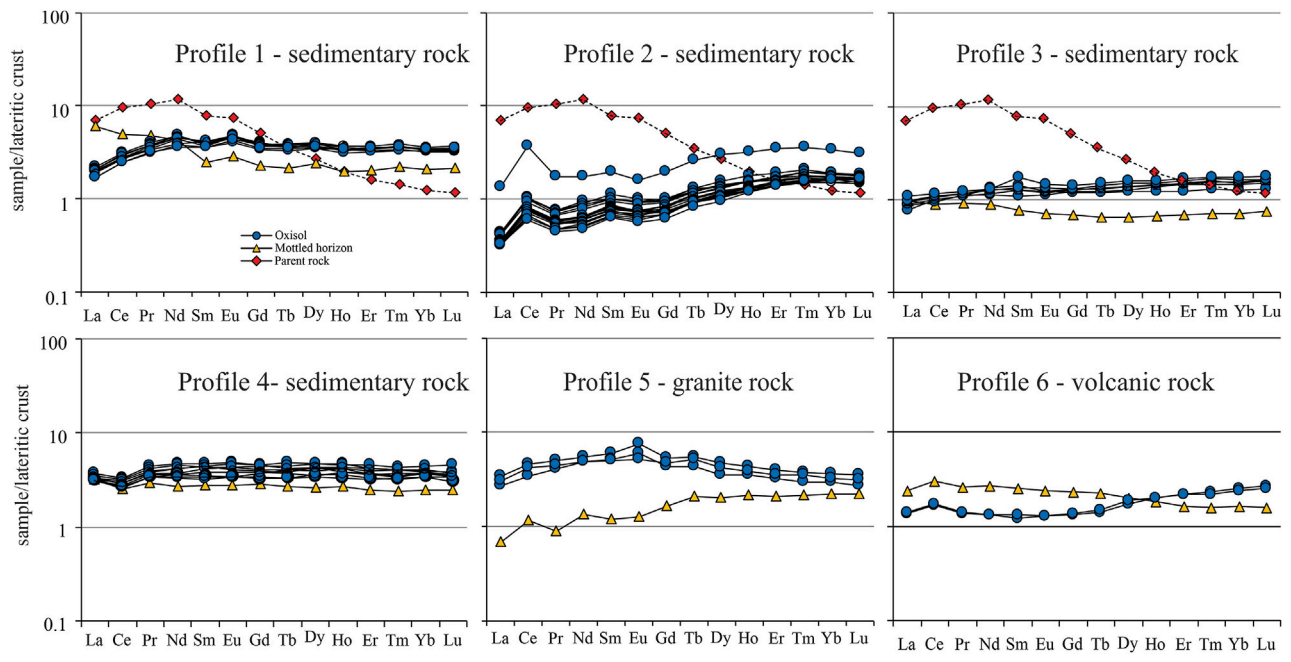

FIGURE 5 | Plot of REE expressed as ppm normalized to the average composition of the duricrust. The Oxisol is enriched in REE and depleted in LREE, except the LREE in profiles 4. Profile 4 also shows a slight positive Ce anomaly.

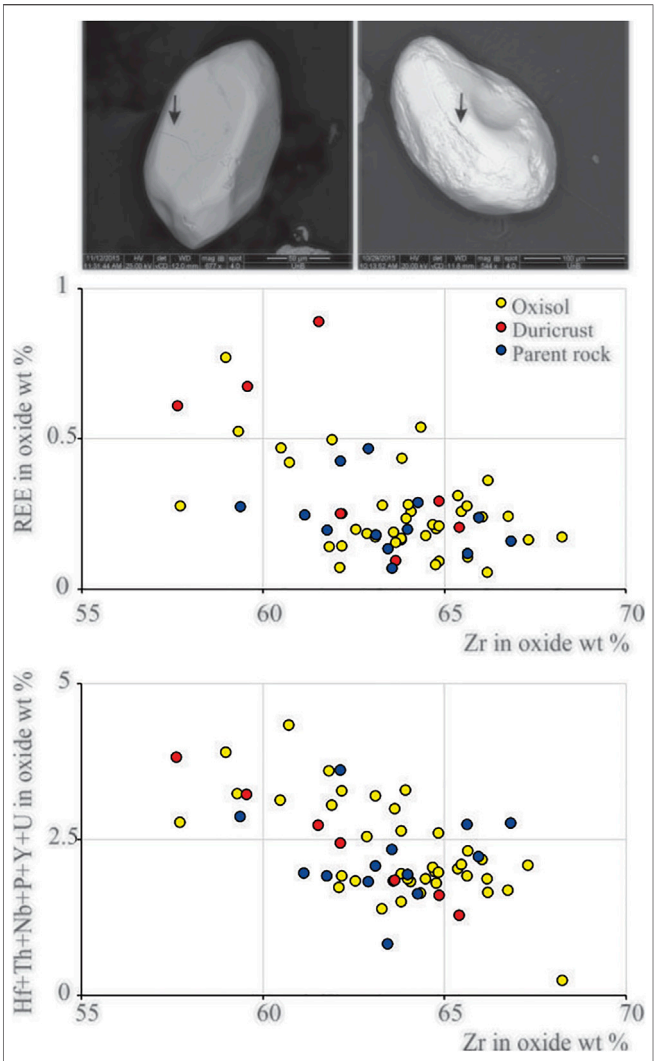

FIGURE 6 | Scanning electron microscope (SEM) images of two zircon grains showing fractures where low-temperature weathering solutions can penetrate changing the Nd system. Plots of REE and Si + Hf + Y + Th + U + Nb + P vs. Zr from EMPA (all elements in oxides concentration and expressed as weight %) of zircon grains of profiles 1 and 2 on the sedimentary Alter do Chão Formation showing the range between the parent rock and the horizons.

digested samples composed mainly of Si-Al and residual minerals, are radiogenic and similar to the respective bulk sample (**Figure 7**).

3.7 Sr and Rb Concentrations and Sr Isotopes

The Sr and Rb concentrations decreased from the parent rock and/or the mottled horizon to the lateritic duricrust (**Table 2**). Toward the top of the Oxisol Rb is close detection limit (<0.1 ppm), although sample 8 m of profile 2 and sample 2.5 m of profile 4 show some anomalously high concentrations causing variabilities in the Rb/Sr ratios (**Figure 8**). In all profiles Sr increases slightly from the lateritic duricrust to the Oxisol and reaches an anomalously high concentration in sample 8 m of profile 2.

The horizons of profiles 1, 2, and 3 are less radiogenic than the parent rock (**Figure 8**), and most of the samples of profiles 5 and 6 are more radiogenic ($^{87}Sr/^{86}Sr$ = 0.74–0.76) than the other profiles samples ($^{87}Sr/^{86}Sr$ 0.715–0.73). Profiles 1 and 2 have highly variable $^{87}Sr/^{86}Sr$ isotope ratios, making the horizons isotopically indistinguishable; however, profiles 3 to 6 show less radiogenic $^{87}Sr/^{86}Sr$ trend toward the top.

4 DISCUSSION

Since Nd and Sr isotope systems vary along the weathering profiles according to the REE and Rb-Sr-bearing mineral composition (e.g., Tripathy et al., 2011 and Jonell et al., 2018), biogeochemistry (e.g., Capo et al., 1998), and atmospheric contributions (e.g., Chabaux et al., 2013; Babechuk et al., 2015), it is necessary to establish well the chemical and mineral compositions relationship among the horizons.

4.1 The Geochemical Signatures of the Weathering Process

The similar SiO_2 and Al_2O_3 contents in the Oxisol in profiles 1, 2, and 5 (**Figure 2**) indicate the coexistence of quartz, kaolinite, and gibbsite; the highest SiO_2 content in profiles 3 and 4 is due to quartz predominance over kaolinite along the profiles, and the highest Al_2O_3 content in profile 6 is a consequence of kaolinite abundance in the mottled horizon and of gibbsite in the Oxisol. These changes in the mineral composition are a consequence of parent rock and the intensity of weathering. In the tropical harsh weathering there is more gibbsite and less quartz.

The Hf, Nb, Ta, Th, TiO_2, Y, Zr, and REE concentrations follow the SiO_2 and/or Al_2O_3 contents across the profiles. Slight variabilities in the Th/Nb, Nb/Y, Zr/Th, Zr/Y, and Th/Y ratios (**Tables 2**, **3**), the Zr/Hf and Nb/Ta ratios of profiles 1, 2, and 3 in the range of the parent rock (**Figure 3**), the $\varepsilon Nd_{(t=0)}$ in the range of Amazon Craton province (**Figure 9**), and Abouchami et al. (2013) ruling out a Saara dust contribution in the study region indicate a progressive *in situ* weathering transformation to all horizons of the profiles. This transformation accumulating residual elements in a long and complex history that can take millions of years (e.g., Chabaux et al., 2013; Guinoiseau et al., 2021) is the typical tropical process that recycled the parent rock developing thick lateritic profiles. This reduced the primary mineral diversity through progressive dissolution and leaching of mobile elements of the mineral species, forming Fe and Al lateritic duricrust and concentrating residual minerals (e.g., Nahon 1991; Horbe and Costa 1999; Retallack, 2010). The *in situ* kaolinite Oxisol accumulation in the top of the profiles was produced by lateritic duricrust pedogenic transformation related to the modern humid conditions and intense Amazon forest plant root activity (e.g., Lucas, 2001; Horbe and Costa, 2005; Costa et al., 2014).

The increase of TiO_2, Zr, and REE concentrations to the top of the profiles (**Tables 2** and **3**) are mostly in rutile, zircon, and REE

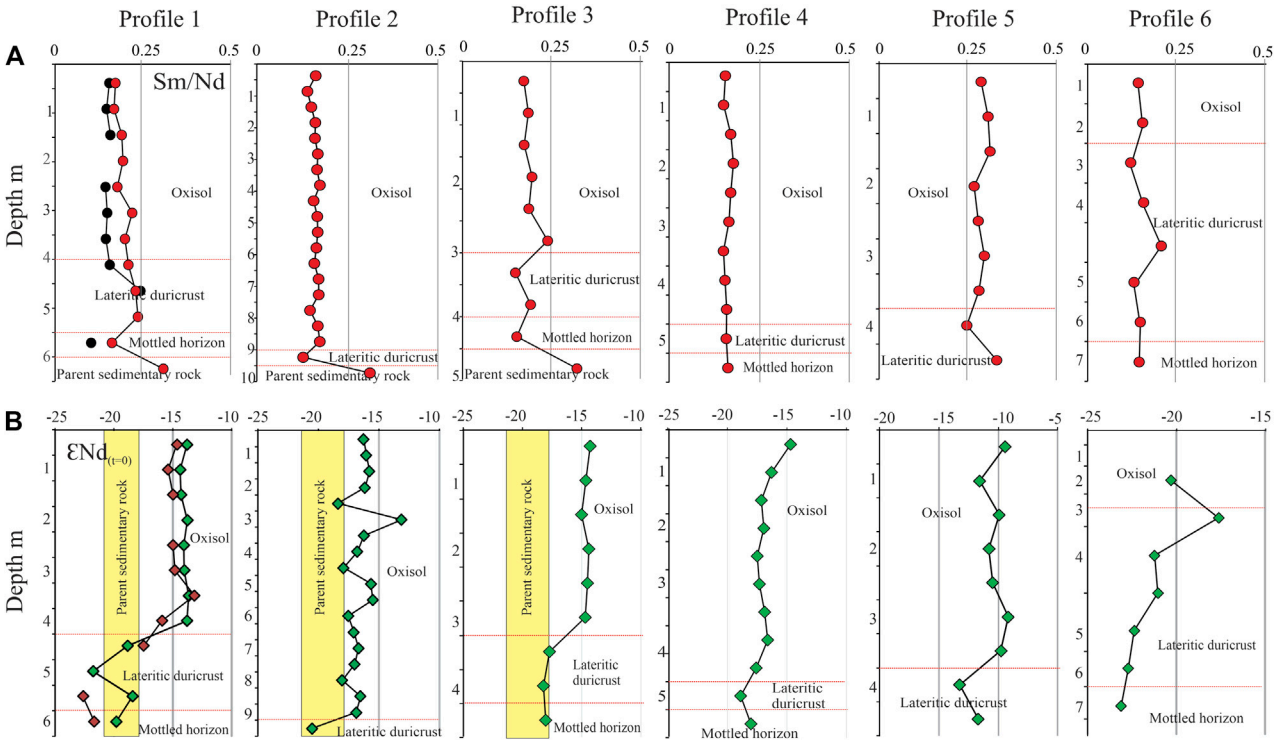

FIGURE 7 | (A): Plot of Sm/Nd ratios in red dots color and **(B)**: Plot of $\varepsilon Nd_{(t=0)}$ in green diamond color in the bulk samples (triacid leaching). In profile 1 the black dots color show the Sm/Nd ratios and the brown diamond color the $\varepsilon Nd_{(t=0)}$) in the aqua regia leaching. The $\varepsilon Nd_{(t=0)}$ of the parent rocks of profiles 1, 2 and 3 are also shown in yellow rectangle. The Sm/Nd ratios are higher in the parent rock of profiles 1–3 do not following the $\varepsilon Nd_{(t=0)}$ that is usually less radiogenic in the parent rock, mottled horizon and lateritic duricrust compared to the much more radiogenic and less variable Oxisol.

TABLE 4 | Sm and Nd concentrations expressed as ppm and Nd and Sr isotopes ratios of profiles 1, 2, and 3 parent rock.

Sample	Sm	Nd	$^{147}Sm/^{144}Nd$	$^{143}Nd/^{144}Nd$	$\varepsilon Nd_{(0)}$	T_{DM}	$^{87}Sr/^{86}Sr$
1	5.468	36.959	0.0894	0.511531 ± 6	−21.59	1.84	0.79469 ± 1
2	1.286	7.781	0.0999	0.511563 ± 21	−20.96	1.97	0.73038 ± 1
3	1.265	7.925	0.0965	0.511527 ± 3	−21.67	1.96	0.73484 ± 2
4	2.099	16.680	0.0761	0.511622 ± 19	−19.82	1.56	0.74319 ± 1
5	0.287	1.300	0.1335	0.511560 ± 13	−21.03	2.83	0.73678 ± 1
6	2.858	17.264	0.1001	0.511611 ± 5	−20.04	1.91	0.73981 ± 1
7	2.328	12.845	0.1096	0.511705 ± 21	−18.20	1.94	0.74306 ± 8
8	4.846	30.805	0.0951	0.511609 ± 6	−20.07	1.83	0.74182 ± 1
9	5.216	34.869	0.0904	0.511627 ± 7	−19.72	1.74	0.74619 ± 1
10	0.992	6.434	0.0932	0.511527 ± 22	−21.67	1.91	0.75204 ± 1
11	3.963	22.833	0.1049	0.511676 ± 13	−18.77	1.90	0.74846 ± 1

minerals that are the typical residual minerals in lateritic profiles. Zircon is a REE-hosted mineral (Belousova et al., 2002; Meyer et al., 2011), since the zircon chemical composition of profiles 1 and 2 indicated up to 0.9% of REE concentration (**Figure 6**) and Zr reached between 1,107 and 3,757 ppm in the Oxisol (**Table 2**), most of the REE content of the profiles could be in the zircon grains. Other possible REE-residual hosted minerals are monazite, xenotime, and florencite, which are stable weathering phosphatic minerals. However, P_2O_5 follows the REE behavior, only between the parent rock and the mottled horizon of the profiles (**Tables 2**, **3**), indicating they are probably related to weatherable apatite and not to residual REE phosphates-bearing minerals. However, small amount of Al phosphate may occur.

Since the $\varepsilon Nd_{(t=0)}$ is related to REE minerals, there are the following possibilities to explain the displacement of REE concentrations and the radiogenic $\varepsilon Nd_{(t=0)}$, especially in the Oxisol (**Figure 9**): 1) authigenic La-cerianite as indicated by the higher REE concentration in the Oxisol and the oxidant weathering condition that allowed the formation of REE oxides

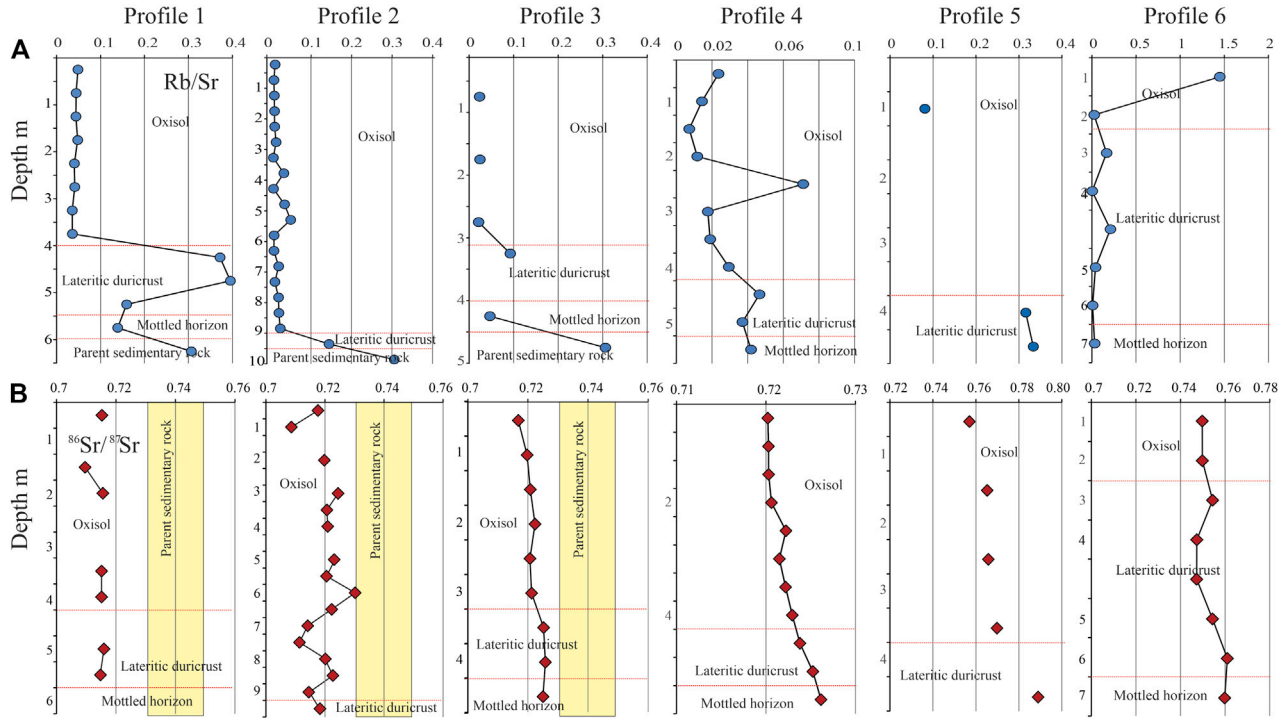

FIGURE 8 | (A): Plot of Rb/Sr in blue dots color and **(B)**: plot of $^{86}Sr/^{87}Sr$ ratios in red diamond color. The $^{86}Sr/^{87}Sr$ values of the parent rocks of profiles 1, 2 and 3 are also shown (yellow rectangle). The Rb/Sr ratios decrease from the parent rock and/or the mottled horizon to the lateritic duricrust. There is a trend to less radiogenic $^{86}Sr/^{87}Sr$ ratios toward the top of the profiles 3–6, whereas in the profiles 1 and 2 the $^{87}Sr/^{86}Sr$ isotope ratios making the horizons isotopically indistinguishable.

after apatite or other REE weathered mineral dissolution (**Table 3**, e.g., Viers and Wasserburg 2004; Zaitsev et al., 2011), 2) higher crystallographic disorder kaolinite in the Oxisol (Guinoiseau et al., 2021) that can sorbed REE (e.g., Yang et al., 2019), and 3) zircon accumulation in consequence of the weathering process (Horbe and Costa, 1999; Jonell et al., 2018). Although cerianite formation is a potential link to Ce/Ce* positive anomaly, it can occur even in samples where Ce anomaly is negative (Ram et al., 2019).

The bauxite and ferruginous lateritic duricrusts that are the most leached horizons of weathering profiles and have lower REE concentration than the other horizons, discard the REE be complexed or adsorbed into Al and Fe inorganic ligands (e.g., Ohlander et al., 1996; Ma et al., 2010; Yang et al., 2019) in these horizons after apatite or other REE weathered mineral dissolution.

4.2 Cerianite, Kaolinite, and Zircon as Controller of REE and Nd Isotope Signatures in the Lateritic Profiles

The probable authigenic cerianite after apatite or other REE weathered mineral dissolution and the formation of disordered kolinite in the acid and oxidant conditions typical of tropical weathering profiles, highlight the possibility that these minerals host the more radiogenic Nd isotopes in the Oxisol after the less radiogenic Nd fraction release (drift of 1–7 $\varepsilon Nd_{(t=0)}$ units, **Figure 9**) in consequence of pedogenic water interaction. Although Nd isotope fractionation in low temperature conditions is not expected, it is reported, for example, in basalt weathering profiles (Ma et al., 2010) and in river water (Andersson et al., 2001), just as it happens in other heavy elements as U (Stirling et al., 2007). On the other hand, the slight drift to further radiogenic $\varepsilon Nd_{(t=0)}$ in the topmost meter of the Oxisol (**Figure 7**, profiles 1, 3, 4, and 5), similar to the drift between the lateritic duricrust and the Oxisol, might indicate superficial REE mobilization effects related to pedogenic solution and vegetation uptake (e.g., Andersson et al., 2001; Aubert et al., 2001; Braun et al., 2017) under the modern humid conditions. Six to eight million years of this process, as indicated (Balan et al., 2005) for Oxisol formation in the region, could cause the radiogenic $\varepsilon Nd_{(t=0)}$ signature of the Oxisol.

Zircon is a residual resistant mineral that retains the low $\varepsilon Nd_{(t=0)}$ ratios of the parent rock and therefore the local province signature of the Amazon craton (Santos et al., 2000; Santos, 2003). The Amazon Craton parent rocks of profiles 5 and 6, and the source of the Paleozoic sedimentary parent rock of profiles 1, 2, 3, and 4 (**Figure 1**). Penetration of low-temperature weathering solutions along fractures, similar to those shown in the studied zircon grains (**Figure 6**), can change U-Pb systems in euhedral zircon grains as reported by Lee and Tromp (1995)

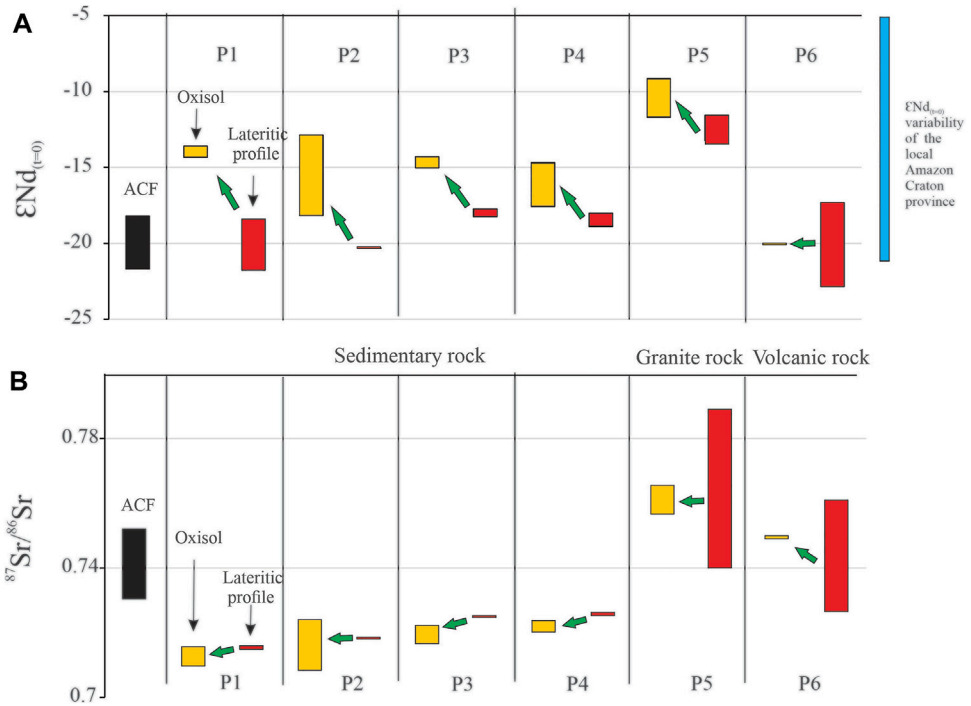

FIGURE 9 | Plot of $\varepsilon Nd_{(t=0)}$ and $^{86}Sr/^{87}Sr$ ratios comparing the variabilities (maximum and minimum values) between the mottled horizon and the lateritic duricrust in red rectangle relative to the Oxisol in orange rectangle in profiles 1 to 6 (P1 to P6). $\varepsilon Nd_{(t=0}$ parent rock variabilities from profiles 1, 2, and 3 in black rectangle. **(A)** Profiles 1 to 3 have similar parent rock, mottled horizon, and lateritic duricrust radiogenic $\varepsilon Nd_{(t=0)}$, and there is an increase in the radiogenic $\varepsilon Nd_{(t=0)}$ to the Oxisols except in P6. **(B)** Profiles 1 to 3 have decreased radiogenic $^{86}Sr/^{87}Sr$ from the parent rock (AFC) to the Oxisol and profile 4 from the mottled horizon and lateritic duricrust to the Oxisol. Profiles 5 and 6 have less variabilities in the Oxisol relative to the mottled horizon and lateritic duricrust.

and Pidgeon et al. (2019). If these solutions also affected the Nd system together the high Zr concentration in the Oxisol, it would be possible for zircon to become a potential source of the further radiogenic $\varepsilon Nd_{(t=0)}$ in the Oxisol after the less radiogenic fraction leaching. The penetrating weathering solutions could also explain the chemical composition of some zircon samples out of the parent rock range in profiles 1 and 2 (**Figure 6**).

Although details of the process that change the Nd system are not well known yet, our investigation indicates a similar effective fractionation degree in the Nd isotopes in the Oxisol profiles (**Figure 9**) related to surficial weathering/pedogenetic process where parent rock composition, atmospheric deposition, or seasonal water saturation dynamics have lower impact. Profile 6 does not follow this behavior very likely because in only one Oxisol sample it was possible to get $\varepsilon Nd_{(t=0)}$ values.

4.3 The Sr Isotope Signatures in the Lateritic Processes

Although there is variability of Sr isotopes especially along profile 2, profiles 3 to 6 show that there is a remarkable progressive transformation caused by the lateritic weathering in the $^{87}Sr/^{86}Sr$ system (**Figure 8**). On the other hand, the $^{87}Sr/^{86}Sr$ ratios higher than >0.74 allow highlighting the influence of K feldspar and mica that are common minerals in the granite and felsic volcanics in determining the more radiogenic isotopic signature of profiles 5 and 6. The weatherability of these minerals and the low capacity to be preserved in sedimentary environment explain the low $^{87}Sr/^{86}Sr$ ratios in the other profiles (**Figure 8**; **Tables 2**, **3**).

The higher capacity of Sr to be hosted in kaolinite (Innocent et al., 1997) explains the Sr concentration in the Oxisol (**Table 2**). However, the decreasing behavior of Rb/Sr and in $^{87}Sr/^{86}Sr$ ratios along most of the profiles highlights two processes. The first one is the leached Sr and Rb making the lower horizons less radiogenic than the parent rocks and the second one is the probable Sr plant returns that increase the Sr concentration in the Oxisol. However, these plant returns that can assimilate the lighter isotopes of Sr (Souza et al., 2010) and the less radiogenic Sr inputs from biogenic aerosol, as well as the lower sea influence in the rainwater of the region (Artaxo et al., 2005; Honório et al., 2010) (Allègre et al., 1996), could explain the further decrease in the $^{87}Sr/^{86}Sr$ ratios. Although Sr and Rb are easily released in the lateritic environment affecting the $^{87}Sr/^{86}Sr$ ratios, the influence of the inherited parent rock minerals is partially retained in the profiles allowing to identify the parent rock signature. Remains and different amounts of Sr weatherable minerals with distinct $^{87}Sr/^{86}Sr$ ratios like biotite, K feldspar,

plagioclase, hornblende, and apatite can also explain the variability in the radiogenic ratios across profile 2.

5 CONCLUSION

The progressive dissolution and leaching of the mobile elements under the harsh tropical chemical weathering, and especially in the Oxisol formed in consequence of the modern pedogenetic humid conditions, not only reduce the primary mineral diversity by concentrating Al and/or Fe oxi-hydroxides, kaolinite, and residual minerals but also change the inherited isotope signatures of primary minerals. However, Nd and Sr systems have distinct behavior. The Sr and Rb leaching makes the weathering profiles progressively less radiogenic, while the *in situ* upward Oxisol formation produces radiogenic Nd fractionation. Four possibilities are indicated together or separately as responsible for the Nd isotopes changes in the Oxisol: cerianite and/or disorder kaolinite authigenic minerals, penetration of low-temperature weathering solutions along zircon fractures, and some superficial REE mobilization related to vegetation uptake. All these possibilities store the radiogenic Nd isotopes fraction relative to the lower horizons. These similar behaviors identified in the six profiles, four from sedimentary rocks and two from igneous rocks, indicate that the radiogenic Nd of the Oxisols was produced in a natural process not related to parent rock, atmospheric deposition, and seasonal water saturation dynamics but related to water interaction. However, the degree of Sr and Nd radiogenie is controlled by the parent rock signature.

DATA AVAILABILITY STATEMENT

The raw data supporting the conclusion of this article will be made available by the authors, without undue reservation.

AUTHOR CONTRIBUTIONS

AH collected the samples and prepared the first draft. ED did the isotopes chemical analysis. MA prepared the samples for microprobe analysis. All the authors discussed the results and participated in the organization of the manuscript.

FUNDING

This research was supported by the CNPq (Conselho Nacional de Desenvolvimento Científico e Tecnológico, grants 620003/2006-8, 150132/2012-3, and 302.618/2016-3) and CLIMAZON (grant 295091).

REFERENCES

Abouchami, W., Näthe, K., Kumar, A., Galer, S. J. G., Jochum, K. P., Williams, E., et al. (2013). Geochemical and Isotopic Characterization of the Bodélé Depression Dust Source and Implications for Transatlantic Dust Transport to the Amazon Basin. *Earth Planet. Sci. Lett.* 380, 112–123. doi:10.1016/j.epsl.2013.08.028

Allègre, C. J., Dupré, B., Négrel, P., and Gaillardet, J. (1996). Sr-Nd-Pb Isotopes Systematics in Amazon and Congo River Systems: Constrain about Erosion Processes. *Chem. Geology.* 131, 93–112. doi:10.1016/0009-2541(96)00028-9

Andersson, P. S., Dahlqvist, R., Ingri, J., and Gustafsson, O. R. (2001). The Isotopic Composition of Nd in a Boreal River: A Reflection of Selective Weathering and Colloidal Transport. *Geochimica et Cosmochimica Acta* 65 (4), 521–527. doi:10.1016/s0016-7037(00)00535-4

Artaxo, P., Gatti, L. V., Leal, A. M. C., Longo, C. M., Freitas, S. R., Lara, L. L., et al. (2005). Química atmosférica na Amazônia: A floresta e as emissões de queimadas controlando a composição da atmosfera amazônica. *Acta Amazônica* 35, 185–196. doi:10.1590/s0044-59672005000200008

Aubert, D., Stille, P., and Probst, A. (2001). REE Fractionation during Granite Weathering and Removal by Waters and Suspended Loads: Sr and Nd Isotopic Evidence. *Geochimica et Cosmochimica Acta* 65, 387–406. doi:10.1016/s0016-7037(00)00546-9

Babechuk, M. G., Widdowson, M., Murphy, M., and Kamber, B. S. (2015). A Combined Y/Ho, High Field Strength Element (HFSE) and Nd Isotope Perspective on basalt Weathering, Deccan Traps, India. *Chem. Geology.* 396, 25–41. doi:10.1016/j.chemgeo.2014.12.017

Balan, E., Allard, T., Fritsch, E., Sélo, M., Falguères, C., Chabaux, F., et al. (2005). Formation and Evolution of Lateritic Profiles in the Middle Amazon basin: Insights from Radiation-Induced Defects in Kaolinite. *Geochimica et Cosmochimica Acta* 69, 2193–2204. doi:10.1016/j.gca.2004.10.028

Bayon, G., German, C. R., Boella, R. M., Milton, J. A., Taylor, R. N., and Nesbitt, R. W. (2002). An Improved Method for Extracting marine Sediment Fractions and its Application to Sr and Nd Isotopic Analysis. *Chem. Geology.* 187, 179–199. doi:10.1016/s0009-2541(01)00416-8

Belousova, E. A., Griffin, W. L., O'Reilly, S. Y., and Fisher N, N. I. (2002). Igneous Zircon: Trace Element Composition as an Indicator of Source Rock Type. *Contrib. Mineralogy Petrol.* 143, 602–622. doi:10.1007/s00410-002-0364-7

Blum, J. D., and Erel, Y. (1997). Rb-Sr Isotope Systematics of a Granite Soil Chronosequences: The Importance of Biotite Weathering. *Geochemica et Cosmochemica Acta* 61, 3193–3204. doi:10.1016/s0016-7037(97)00148-8

Boulangé, B., and Carvalho, A. (1997). "The bauxite of Porto Trombetas," in *Brazilian Bauxites, USP/FAPESP/ORSTOM, Brazil.* Editors A. Carvalho, B. Boulangé, A. J. Melfi, and Y. Lucas, 55–73.

Braun, J. J., Pagel, M., Herbillon, A., and Rosins, C. (1993). Mobilization and Redistribution of REE and Thorium in a Syenitic Lateritic Profile: A Mass Balance Study. *Geochimica et Cosmochimica Acta* 51, 4419–4434. doi:10.1016/0016-7037(93)90492-f

Braun, J. J., Pagel, M., Muller, J. P., Bilong, A. M., and Guillet, B. (1990). Cerium Anomalies in Lateritic Profiles. *Geochimica et Cosmochimica Acta* 54, 781–795. doi:10.1016/0016-7037(90)90373-s

Braun, J. J., Riotte, J., Battacharya, S., Violette, A., Prunier, J., Bouvier, V., et al. (2017). REY-Th-U Solute Dynamics in the Critical Zone: Combined Influence of Chemical Weathering, Atmospheric Deposit Leaching, and Vegetation Cycling (Mule Hole Watershed, South India). *Geochem. Geophys. Geosystems* 18, 4409–4425. doi:10.1002/2017gc007158

Cao, X., Chen, Y., Wang, X., and Deng, X. (2001). Effects of Redox Potential and pH Value on the Release of Rare Earth Elements from Soil. *Chemosphere* 44, 655–661. doi:10.1016/s0045-6535(00)00492-6

Capo, R. C., Stewart, B. W., and Chadwick, O. A. (1998). Strontium Isotopes as Tracers of Ecosystem Process: Theory and Methods. *Geoderma* 82, 197–225. doi:10.1016/s0016-7061(97)00102-x

Chabaux, F., Blaes, E., Stille, P., Roupert, R. C., Pelt, E., Dosseto, A., et al. (2013). Regolith Formation Rate from U-Series Nuclides: Implications from the Study of a Spheroidal Weathering Profile in the Rio Icacos Watershed (Puerto Rico). *Geochimica et Cosmochimica Acta* 100, 73–95. doi:10.1016/j.gca.2012.09.037

Costa, M. L., Cruz, G. S., Almeida, H. D. F., and Poellmann, H. (2014). On the Geology, Mineralogy and Geochemistry of the bauxite-bearing Regolith in the Lower Amazon basin: Evidence of Genetic Relationships. *J. Geochemical Exploration* 146, 58–74. doi:10.1016/j.gexplo.2014.07.021

Cunha, P. R. C., Gonzaga, F. G., Coutinho, L. F. C., and Feijó, F. J. (1994). Bacia Do Amazonas. *Boletim Geociências da Petrobras* 8, 47–55.

Daemon, R. F., and Contreiras, C. J. A. (1971). "Zoneamento palinológico da bacia Do Amazonas," in *Congresso Brasileiro de Geologia, 25º, São Paulo, 1971* (Anais. São Paulo: Sociedade Brasileira de Geologia), 3, 79–88.

Daemon, R. F. (1975). *Contribuição à datação da Formacão Alter do Chão, bacia do Amazonas*, 5. Rio de Janeiro: Revista Brasileira de Geociências, 58–84.

Gioia, S. M. C. L., and Pimentel, M. M. (2000). The Sm–Nd Isotopic Method in the Geochronology Laboratory of the University of Brasília. *Anais da Academia Brasileira de Ciências* 72, 219–245. doi:10.1590/s0001-37652000000200009

Guinoiseau, D., Fekiacova, Z., Allard, T., Druhan, J. L., Balan, E., and Bouchez, J. (2021). Tropical Weathering History Recorded in the Silicon Isotopes of Lateritic Weathering Profiles. *Geophys. Res. Lett.* 48, e2021GL092957. doi:10.1029/2021gl092957

Harlavan, Y., Erel, Y., and Blum, J. D. (2009). The Coupled Release of REE and Pb to the Soil Labile Pool with Time by Weathering of Accessory Phases, Wind River Mountains, WY. *Geochimica and Cosmochimica Acta* 73, 320–336. doi:10.1016/j.gca.2008.11.002

Henderson, P. (1986). *Inorganic Geochemistry*. Oxford: Pergamon Press, 353.

Honório, B. A. D., Horbe, A. M. C., and Seyler, P. (2010). Chemical Composition of Rainwater in Western Amazon — Brazil. *Atmos. Res.* 98, 416–425. doi:10.1016/j.atmosres.2010.08.001

Horbe, A. M. C., and Anand, R. (2011). Bauxite on Igneous Rocks from Amazon and Southwestern of Australia: Implication for Weathering Process. *J. Geochemical Exploration* 111, 1–12. doi:10.1016/j.gexplo.2011.06.003

Horbe, A. M. C., and Costa, M. L. (1999). Geochemical Evolution of Lateritic Sn. Zr. Th. Nb. Y and REE - Bearing Ore Body Derived from Apogranite: the Case of Pitinga. Amazonas - Brazil. *J. Geochemical Exploration* 66, 339–351. doi:10.1016/s0375-6742(99)00002-3

Horbe, A. M. C., and Costa, M. L. (2005). Lateritic Crusts and Related Oxisols in Eastern Brazilian Amazon. *Geoderma* 126, 225–239. doi:10.1016/j.geoderma.2004.09.011

Horbe, A. M. C. (2011). Oxygen and Hydrogen Isotopes in Pedogenic Minerals – Implications for Paleoclimate Evolution in Amazon during the Cenozoic. *Geoderma* 163, 178–184. doi:10.1016/j.geoderma.2011.03.017

Hoskin, P. W. O., and Schaltegger, U. (2003). The Composition of Zircon and Igneous and Metamorphic Petrogenesis. *Rev. Mineralogy Geochem.* 53, 27–62. doi:10.1515/9781501509322-005

Innocent, C., Michard, A., Malengreau, N., Loubet, M., Noack, Y., Benedetti, M., et al. (1997). Sr Isotopic Evidence for Ion-Exchange Buffering in Tropical Laterites from the Paraná, Brazil. *Chem. Geology.* 136, 219–232. doi:10.1016/s0009-2541(96)00145-3

Jacobsen, S. B., and Wasserburg, G. J. (1980). Sm–Nd Isotopic Evolution of Chondrites. *Earth Planet. Sci. Lett.* 50, 139–155. doi:10.1016/0012-821x(80)90125-9

Jonell, T. N., Li, Y., Blusztajn, J., Giosan, L., and Clift, P. D. (2018). Signal or Noise? Isolating Grain Size Effects on Nd and Sr Isotope Variability in Indus delta Sediment Provenance. *Chem. Geology.* 485, 56–73. doi:10.1016/j.chemgeo.2018.03.036

Laveuf, C., and Cornu, S. (2009). A Review on the Potentiality of Rare Earth Elements to Trace Pedogenetic Processes. *Geoderma* 154, 1–12. doi:10.1016/j.geoderma.2009.10.002

Lee, J. K. W., and Tromp, J. (1995). Self-induced Fracture Generation in Zircon. *J. Geophys. Res.* 100 (B917), 753-17–770. doi:10.1029/95jb01682

Liu, X-M., Rudnick, R. L., McDonough, W. F., and Cummings, M. L. (2013). Influence of Chemical Weathering on the Composition of the continental Crust: Insights from Li and Nd Isotopes in bauxite Profiles Developed on Columbia River Basalts. *Geochimica et Cosmochimica Acta* 115, 73–91. doi:10.1016/j.gca.2013.03.043

Lucas, Y. (1997). in *The bauxite of Juriti*. Editors A. Carvalho, B. Boulangé, A. J. Melfi, and Y. B. Lucasbauxites (USP/FAPESP/ORSTOM. Brazil), 107–136. doi:10.1097/00042307-199703000-00010

Lucas, Y. (2001). The Role of Plants in Controlling Rates and Products of Weathering: Importance of Biological Pumping. *Annu. Rev. Earth Planet. Sci.* 29, 135–163. doi:10.1146/annurev.earth.29.1.135

Ma, J., Wei, G., Xu, Y., and Long, W. (2010). Variations of Sr-Nd-Hf Isotopic Systematics in basalt during Intensive Weathering. *Chem. Geology.* 269, 376–385. doi:10.1016/j.chemgeo.2009.10.012

MacFarlane, A. W., Danielson, A., Holland, H. D., and Jacobsen, S. B. (1994). REE Chemistry and Sm-Nd Systematics of Late Archean Weathering Profiles in the Fortescue Group, Western Australia. *Geochimica et Cosmochimica Acta* 58, 1777–1794. doi:10.1016/0016-7037(94)90536-3

McDaniel, D. K., Hemming, S. R., McLennan, S. M., and Hanson, G. N. (1994). Resetting of Neodymium Isotopes and Redistribution of REE during Sedimentary Processes: The Early Proterozoic Chelmsford Formation, Sudbury Basin, Ontario, Canada. *Geochimica et Cosmochimica Acta* 58, 931–941. doi:10.1016/0016-7037(94)90516-9

Meyer, M., John, T., Brandt, S., and Klemd, R. (2011). Trace Element Composition of Rutile and the Application of Zr-In-Rutile Thermometry to UHT Metamorphism (Epupa Complex, NW Namibia). *Lithos* 126, 388–401. doi:10.1016/j.lithos.2011.07.013

Minarik, L., Anna, Z., Bendlb, J., Skrivan, P., and St'astn, M. (1998). The Behaviour of Rare-Earth Elements and Y during the Rock Weathering and Soil Formation in the Rıcany Granite Massif, Central Bohemia. *Sci. Total Environ.* 215, 101–111.

Moragues-Quiroga, C., Juilleret, J., Gourdol, L., Pelt, E., Perrone, T., Aubert, A., et al. (2017). Genesis and Evolution of Regoliths: Evidence from Trace and Major Elements and Sr-Nd-Pb-U Isotopes. *Catena* 149, 185–198. doi:10.1016/j.catena.2016.09.015

Nahon, D. B. (1991). Self-organization in Chemical Lateritic Weathering. *Geoderma* 51, 5–13. doi:10.1016/0016-7061(91)90063-y

Negrel, Ph., Guerrot, C., Cocherie, A., Azaroual, M., Brach, M., and Fouillac, C. (2000). Rare Earth Elements, Neodymium and Strontium Isotopic Systematics in mineral Waters: Evidence from the Massif Central, France. *Appl. Geochem.* 15, 1345–1367. doi:10.1016/s0883-2927(00)00008-1

Ohlander, B., Ingri, J., Land, M., and Schoberg, H. (2000). Change of Sm-Nd Isotope Composition during Weathering of till. *Geochemical et Cosmochemical Acta* 64, 813–820. doi:10.1016/s0016-7037(99)00365-8

Ohlander, B., Land, M., Ingri, J., and Widerlund, A. (1996). Mobility of Rare Earth Elements during Weathering of till in Northern Sweden. *Appl. Geochem.* 1, 93–99. doi:10.1016/0883-2927(95)00044-5

Pereira, V. P., Conceição, R. V., Formoso, M. L. L., and Pires, A. C. (2005). Alteration of Perovskite to Anatase in Silica-Under Saturated Rocks of the Catalão-I Carbonatite Complex, Brazil: a Raman Study. *Revista Brasileira de Geociências* 35, 239–244. doi:10.25249/0375-7536.2005352239244

Pidgeon, R. T., Nemchin, A. A., Roberts, M. P., Whitehouse, M. J., and Bellucci, j. J. (2019). The Accumulation of Non-formula Elements in Zircons during Weathering: Ancient Zircons from the Jack Hills, Western Australia. *Chem. Geology.* 530, 119310. doi:10.1016/j.chemgeo.2019.119310

Ram, R., Becker, M., Brugger, J., Etschmann, B., Burcher-Jones, C., Howard, D., et al. (2019). Characterisation of a Rare Earth Element- and Zirconium-Bearing Ion Adsorption clay deposit in Madagascar. *Chem. Geology.* 522, 93–107. doi:10.1016/j.chemgeo.2019.05.011

Retallack, G. J. (2010). Lateritization and Bauxitization Events. *Econ. Geology.* 105, 655–667. doi:10.2113/gsecongeo.105.3.655

Santoro, A.., Held, A., Linsinger, T. P. J., and Ricci, A. P. M. (2017). Comparison of Total and Aqua Regia Extractability of Heavy Metals in Sewage Sludge: The Case Study of a Certified Reference Material. *Trends Anal. Chem.* 89, 34–40. doi:10.1016/j.trac.2017.01.010

Santos, J. O. S., Hartmann, L. A., Gaudette, H. E., Groves, D. I., Mc Naughton, N. J., and Fletcher, I. R. (2000). A New Understanding of the Provinces of the Amazon Craton Based on Integration of Field Mapping and U-Pb and Sm-Nd Geochronology. *Gondwana Res.* 3, 453–488. doi:10.1016/s1342-937x(05)70755-3

Santos, J. O. S. (2003). "Geotectonics of the Guyana and Central Brazilian Shields," in *Geology, Tectonics, and Mineral Resources of Brazil, Text, Maps and GIS: Brasília, Brazil, Companhia de Pesquisa de Recursos Minerais*. Editors L. A. Bizzi, C. Schobbenhaus, R. M. Vidotti, and J. H. Gonçalves, 169–226. ISBN 85-230-0790-3.

Santos, R. V., Sondag, F., Cochonneau, G., Lagane, C., Brunet, P., Hattingh, K., et al. (2014). "Source Area and Seasonal $^{87}Sr/^{86}Sr$ Variations in Rivers of the Amazon basin," in *Hydrological Process*. (Published online in Wiley Online Library).

Silva, A. J. P., Lopes, R. C., Vasconcelos, A. M., and Bahia, R. B. C. (20032003). "Bacias Sedimentares Paleozóicas e Meso-Cenozóicas Interiores," in *Geologia, Tectônica e Recursos Minerais do Brasil, Capítulo II*. Editors L. A. Bizzi, C. Schobbenhaus, R. M. Vidotti, and J. H. Gonçalves (Brasília: CPRM), 55–85. ISBN 85-230-0790-3, 674).

Souza, G. F., Reynolds, B. C., Kiczka, M., and Bourdon, B. (2010). Evidence for Mass-dependent Isotopic Fractionation of Strontium in a Glaciated Granitic Watershed. *Geochimica et Cosmochimica Acta* 74, 2996–2614. doi:10.1016/j.gca.2010.02.012

Stewart, B. W., Capo, R. C., and Chadwick, O. A. (1998). Quantitative Strontium Isotope Models for Weathering, Pedogenesis and Biogeochemical Cycling. *Geoderma* 82, 173–195. doi:10.1016/s0016-7061(97)00101-8

Stirling, C. H., Andersen, M. B., Potter, E-K., and Halliday, A. N. (2007). Low-temperature Isotopic Fractionation of Uranium. *Earth Planet. Sci. Lett.* 264, 208–225. doi:10.1016/j.epsl.2007.09.019

Su, N., Yang, S., Guo1, Y., Yue, W., Wang, X., Yin, P., et al. (2017). Revisit of Rare Earth Element Fractionation during Chemical Weathering and River Sediment Transport. *Geochem. Geophys. Geosystems* 18, 935–955. doi:10.1002/2016gc006659

Tardy, Y., and Roquin, C. (1998). *Dérive des continents Paléoclimats at alterations tropicales*. Orléans, FranceBRGM, 473.

Taylor, S. R., and McLenann, S. M. (1985). *The Continental Crust its Composition and Evolution*. Oxford: Blackwell Scientific Publications, 312.

Thieblemont, D., Guerrot, C., Negrel, Ph., Braucher, R., Bourles, D. L., and Thieblemont, R. (2014). Nd-isotope Evidence for the Distal Provenance of the Historical (C. <3000 BP) Lateritic Surface Cover Underlying the Equatorial forest. *Gabon (Western Africa)* 15, 177–192. doi:10.1016/j.aeolia.2014.06.002

Tripathy, G. R., Singh, S. K., and Krishnaswami, M., S. (2011). "Sr and Nd Isotopes as Tracers of Chemical and Physical Erosion Baskaran," in *Handbook of Environmental Isotope Geochemistry, Advances in Isotope Geochemistry* (Springer-Verlag Berlin Heidelberg), 521–552. doi:10.1007/978-3-642-10637-8_26

Tyler, G. (2004). Rare Earth Elements in Oxisol and Plant Systems – A Review. *Plant and Oxisol* 267, 191–206. doi:10.1007/s11104-005-4888-2

Velbel, M. (1999). Bond Strength and the Relative Weathering Rates of Simple Orthosilicates. *Am. J. Sci.* 299, 679–696. doi:10.2475/ajs.299.7-9.679

Viers, J., and Wasserburg, G. J. (2004). Behavior of Sm and Nd in a Lateritic Soil Profile. *Geochimica et Cosmochimica Acta* 68, 2043–2054. doi:10.1016/j.gca.2003.10.034

Wei, X., Wang, S., Ji, H., and Shi, Z. (2018). Strontium Isotopes Reveal Weathering Processes in Lateritic Covers in Southern China with Implications for Paleogeographic Reconstructions. *PLoS ONE* 13, e0191780. doi:10.1371/journal.pone.0191780

West, A. J., Galy, A., and Bickle, M. (2005). Tectonic and Climatic Controls on Silicate Weathering. *Earth Planet. Sci. Lett.* 235, 211–228. doi:10.1016/j.epsl.2005.03.020

Wood, S. A. (1990). The Aqueous Geochemistry of the Rare-Earth Elements and Yttrium 1. Review of Available Low-Temperature Data for Inorganic Complexes and the Inorganic REE Speciation of Natural Waters. *Chem. Geology.* 82, 159–186. doi:10.1016/0009-2541(90)90080-q

Yang, M., Liang, X., Ma, L., Huang, J., He, H., and Zhu, J. (2019). Adsorption of REEs on Kaolinite and Halloysite: A Link to the REE Distribution on Clays in the Weathering Crust of Granite. *Chem. Geology.* 525, 210–217. doi:10.1016/j.chemgeo.2019.07.024

Zaitsev, A. N., Chakhmouradian, A. R., Siidra, O. I., Spratt, J., Williams, C. T., Stanley, C. J., et al. (2011). Fluorine-, Yttrium- and Lanthanide-Rich cerianite-(Ce) from Carbonatitic Rocks of the Kerimasi Volcano and Surrounding Explosion Craters, Gregory Rift, Northern Tanzania. *Mineralogical Mag.* 75, 2813–2822. doi:10.1180/minmag.2011.075.6.2813

Conflict of Interest: The authors declare that the research was conducted in the absence of any commercial or financial relationships that could be construed as a potential conflict of interest.

Publisher's Note: All claims expressed in this article are solely those of the authors and do not necessarily represent those of their affiliated organizations or those of the publisher, the editors and the reviewers. Any product that may be evaluated in this article, or claim that may be made by its manufacturer, is not guaranteed or endorsed by the publisher.

Copyright © 2022 Horbe, Albuquerque and Dantas. This is an open-access article distributed under the terms of the Creative Commons Attribution License (CC BY). The use, distribution or reproduction in other forums is permitted, provided the original author(s) and the copyright owner(s) are credited and that the original publication in this journal is cited, in accordance with accepted academic practice. No use, distribution or reproduction is permitted which does not comply with these terms.